A Problematic Tyrannosaurid (Dinosauria: Theropoda) Skeleton and its Implications for Tyrannosaurid Diversity in the Horseshoe Canyon Formation (Upper Cretaceous) of Alberta

JORDAN C. MALLON [1,2*] JONATHAN R. BURA,[3] DIRK SCHUMANN,[4] AND PHILIP J. CURRIE [5]

[1]Beaty Centre for Species Discovery and Palaeobiology Section, Canadian Museum of Nature, Ottawa, Ontario, Canada
[2]Department of Earth Sciences, Carleton University, Ottawa, Ontario, Canada
[3]Department of Earth and Environmental Sciences, University of Ottawa, Ottawa, Ontario, Canada
[4]Fibics Incorporated, Ottawa, Ontario, Canada
[5]Department of Biological Sciences, University of Alberta, Edmonton, Alberta, Canada

ABSTRACT

Several published censuses have noted the presence of two tyrannosaurids, *Daspletosaurus* sp. and *Albertosaurus sarcophagus*, within the Upper Cretaceous Horseshoe Canyon Formation of Alberta. Although *A. sarcophagus* is known from more than a dozen major discoveries in these strata, *Daspletosaurus* sp. is known from just a single problematic skeleton (lacking most of the skull) of a young individual. Here we describe and figure this skeleton, and marshal a variety of osteohistologic, morphometric, and phylogenetic methods to accurately determine its taxonomic status. Although none of these methods individually provides convincing evidence regarding the affinities of the specimen, together (and including other historical and biostratigraphic considerations) they strongly imply that the skeleton instead pertains to a young *A. sarcophagus*. In this way, we show that only a single species of tyrannosaurid is definitively present in the Horseshoe Canyon Formation, greatly simplifying interpretations of tyrannosaurid evolution and ecology in this setting. Anat Rec, 303:673–690, 2020. © 2019 The Authors. *The Anatomical Record* published by Wiley Periodicals, Inc. on behalf of American Association of Anatomists.

Key words: Tyrannosauridae; osteohistology; taxonomy; Horseshoe Canyon Formation; morphometrics

Additional Supporting Information may be found in the online version of this article.

Abbreviations: CMN = Canadian Museum of Nature, Ottawa, Ontario; ROM = Royal Ontario Museum, Toronto, Ontario; TMP = Royal Tyrrell Museum of Palaeontology, Drumheller, Alberta

Grant sponsor: Natural Sciences and Engineering Research Council of Canada; Grant number: RGPIN-2017-06356.

*Correspondence to: Beaty Centre for Species Discovery and Palaeobiology Section, Canadian Museum of Nature, PO Box 3443, Station D, Ottawa K1P 6P4, ON, Canada. Fax: 613-364-4027 E-mail: jmallon@nature.ca

Received 22 May 2018; Revised 30 November 2018; Accepted 11 January 2019.

DOI: 10.1002/ar.24199
Published online 29 June 2019 in Wiley Online Library (wileyonlinelibrary.com).

In 1926, Charles M. Sternberg discovered the partial skeleton of an immature tyrannosaurid (CMN 11315; Fig. 1) within a sandstone on the south bank of the Red Deer River, Alberta, upstream of the Tolman Bridge (SW 1/8, Section 20, Township 34, Range 21, west of the 4th meridian). These coordinates place the specimen within the lower Maastrichtian Tolman Member of the Horseshoe Canyon Formation (Eberth et al., 2013). Sternberg initially attributed the specimen to *Albertosaurus sarcophagus* (1926 field notes, CMN archives), likely based on the fact that no other tyrannosaurids had yet been described from those strata. However, Russell (1970) later reassigned CMN 11315 to *Daspletosaurus cf. D. torosus*, based on the proportions of the forelimb, ilium, femur, and on the curvature of the claw of the first manual digit. The holotype of *D. torosus* otherwise comes from the middle Campanian Oldman Formation of Alberta.

The classification of CMN 11315 as *D. torosus* has become widely cited in the literature (Makovicky and Currie, 1998; Currie, 2003a; Claessens, 2004; Nesbitt et al., 2009), although others (Madsen Jr, 1974; Holtz Jr, 2000; Currie, 2003b; Eberth et al., 2013; Persons IV and Currie, 2016) have accepted Sternberg's original assessment of the specimen as *A. sarcophagus.* The reasons for this disagreement are unclear, but in all likelihood reflect the fact that diagnostic skeletal characters are often not expressed in immature individuals (Hone et al., 2016). Importantly, several censuses (Russell, 1984; Carpenter, 1992; Ryan and Russell, 2001; Weishampel et al., 2004a; Weishampel et al., 2004b; Brown et al., 2015) have listed both *A. sarcophagus* and *Daspletosaurus* sp. as present in the Horseshoe Canyon Formation, presumably on the basis of Russell's (1970) initial assessment, which is the only published instance citing evidence for *Daspletosaurus* in the formation.

The ramifications concerning the identity of CMN 11315 are not insignificant. First, if the specimen truly is *Daspletosaurus* sp., it would provide evidence for the presence of two co-occurring large apex-predators within the Horseshoe Canyon Formation, which introduces a suite of palaeoecological complications (Farlow and Planka, 2002). Second, although *A. sarcophagus* is typically restricted to the Horseshoe Canyon Formation (Carr, 2010; Tanke and Currie, 2010), *Daspletosaurus* spp. are otherwise known only from the middle to late Campanian Oldman, Dinosaur Park, and Two Medicine formations in Alberta and Montana (Currie, 2005; Currie et al., 2005; Carr et al., 2017). Thus, if CMN 11315 is attributable to *Daspletosaurus* sp., this would mean a temporal range extension of up to ~3.5 million years for the genus. Establishing the precise identity of this specimen is therefore of great interest, given the potential ecological and evolutionary implications. We do this by first describing and figuring the specimen in some detail, and by further applying a combination of osteohistologic, morphometric, and phylogenetic analyses.

Fig. 1. The disarticulated partial skeleton of CMN 11315 as discovered by C. M. Sternberg in 1926 (CMN neg. 67946). Although the bones are disarticulated, they remain ordered from cranial (right) to caudal (left).

DESCRIPTION OF CMN 11315

The description that follows is not exhaustive, and focuses primarily on those differences between CMN 11315 and other tyrannosaurids. Detailed descriptions of tyrannosaurid skulls are common (e.g., Carr, 1999, 2010; Hurum and Sabath, 2003; Currie, 2003b), and exhaustive treatments of postcrania can be found in Lambe (1917), Parks (1928), Brochu (2003), and Brusatte et al. (2012). The forelimb is described here in greater detail, given that it is often missing in tyrannosaurid specimens, and in light of the interest it has garnered concerning its potential uses (or lack thereof) (Vance, 1989; Carpenter and Smith, 2001; Carpenter, 2002; Lipkin and Carpenter, 2008). Anatomical reference planes for individual elements follow Brochu (2003). General measurements of the various skeletal elements are given in Table 1.

Skull

The skull is incomplete, being represented by just the few bones described below. Evidently, it had mostly eroded away before it could be collected.

The triradiate quadratojugal (Fig. 2A–C) is like that of albertosaurines, and unlike that of *Daspletosaurus* spp. and other tyrannosaurines, in several ways (Currie, 2003b; Carr et al., 2017). First, the wing-like dorsal process is greatly expanded, creating an elongate dorsal contact for the squamosal. Second, the thickened ridge that runs along the rostral surface of the dorsal process attenuates dorsally, and does not meet the squamosal contact. Third, the dorsal contact surface for the jugal along the rostral process of the quadratojugal does not approach the posteroventral corner of the infratemporal fenestra. This process appears to taper rostrally, again as in albertosaurines, but the bone is obviously damaged in this region. There is a small (~4 mm) foramen that perforates the center of the fossa on the dorsal process. This foramen has not been described elsewhere in a tyrannosaurid, but it is variably present in *Albertosaurus sarcophagus* (present: TMP 1981.010.0001, TMP 1985.098.0001; absent: TMP 1998.063.0084). The foramen is distinct from the quadratojugal pneumatopore seen in *Daspletosaurus horneri* and *Nanotyrannus lancensis*, which occurs lower on the lateral surface of the dorsal process, beyond the bounds of the fossa (Larson, 2013; Carr et al., 2017).

The quadrate (Fig. 2C–F) is of typical tyrannosaurid construction, being vaguely P-shaped in outline, and sporting a large fenestra laterally. The fenestra is displaced from the jaw joint by more than two times the height of the quadrate condyles, a condition common in

TABLE 1. Measurements for CMN 11315

Measure	Value (mm)
Left quadrate height	164
Left quadratojugal foramen height	37.2
Left dentary maximum height	65
Left scapula-coracoid length	580
Left scapular blade length	470
Left scapula shaft width	32.7
Left scapula distal width	85
Left coracoid height	116.5
Furcula width	180
Left humerus length	222
Left humerus proximal width	47.4
Left humerus transverse shaft width	25.3
Left humerus distal width	38.3
Left radius length	96.2
Left radius proximal width	18.6
Left radius transverse shaft width	13.1
Left radius distal width	19.3
Left ulna length (including olecranon)	119.5
Left ulna proximal width	30.4
Left ulna anteroposterior shaft width	13.6
Left ulna distal width	21
Left metacarpal I length	35.7
Left metacarpal II length	61.5
Left metacarpal III length	40
Left manual phalanx I-1 length	58
Left manual phalanx I-2 length (straight)	54.5
Left manual phalanx I-2 length (outside curve)	57
Left manual phalanx II-1 length	29
Left manual phalanx II-2 length	40
Left manual phalanx II-3 length (straight)	54
Left manual phalanx II-3 length (outside curve)	58
Left ilium length	675
Left ilium height over pubic peduncle	325
Pubis length	560*
Pubic boot length	360
Left ischium length	495
Femur length	680a
Femur proximal width	120a
Femur shaft width (anteroposterior)	66a
Femur shaft width (transverse)	112a
Femur minimum shaft circumference	314a
Femur distal width	124a
Tibia length	690a
Right tibia-astragalus length	720
Tibia proximal width	150a
Tibia transverse shaft width	62a
Tibia distal width	155a
Fibula length	630a
Fibula proximal width	130a
Fibula shaft width	27a
Fibula distal width	39a
Astragalus height	190a
Astragalus width	137a
Calcaneum maximum height	61a
Calcaneum width	14a
Metatarsal I length	73.5a
Metatarsal II length	410a
Metatarsal III length	445a
Metatarsal IV length	422a
Metatarsal V length	165
Phalanx I-1 length	71
Phalanx II-1 length	118
Phalanx II-2 length	80.6
Phalanx II-3 length (straight)	96
Phalanx II-3 length (outside curve)	110
Phalanx III-1 length	128
Phalanx III-2 length	81.5
Phalanx III-3 length	63
Phalanx III-4 length (straight)	79
Phalanx III-4 length (outside curve)	89
Phalanx IV-1 length	78
Phalanx IV-2 length	61
Phalanx IV-3 length	41
Phalanx IV-4 length	28
Phalanx IV-5 length (straight)	66
Phalanx IV-5 length (outside curve)	73

Asterisk (*) indicates estimated value. Letter 'a' indicates averaged length (between right and left sides).

early tyrannosauroids and some tyrannosaurids (e.g., *D. horneri* and *Teratophoneus curriei*) (Loewen et al., 2013). The pterygoid ala is posteromedially excavated by a deep fossa, a condition common with *A. sarcophagus* and *Bistahieversor sealeyi* (Loewen et al., 2013).

The rostral portion of the dentary is preserved (Fig. 3), as well as pieces of the more caudal region; however, the latter are too fragmentary to be of diagnostic value. The rostral margin of the dentary is straight and faces anteroventrally at an angle of approximately 45 degrees relative to the horizontal dorsal margin, and in this way is reminiscent of *A. sarcophagus* and *Tyrannosaurus rex*; the rostral margin is rounded in *D. torosus*. However, CMN 11315 is unlike *A. sarcophagus* and *T. rex* in that the transition between the rostral and ventral margins of the dentary occurs below the first and second alveolus, as it does in *D. torosus* (Carr and Williamson, 2010). The confluence of the rostral and ventral margins of the dentary is marked by a weakly developed "chin" that is seen in most other tyrannosaurids (Brusatte et al., 2010). The chin is absent in the juvenile "*Raptorex kriegsteini*" (=*Tarbosaurus bataar*). Medially, the surface of the dentary symphysis is smooth as in albertosaurines and some more primitive tyrannosauroids; it is not as rugose as in tyrannosaurines (Brusatte et al., 2010).

Gastralia

A portion of the gastral cuirass is preserved, consisting of 12 free ribs from the left side and nine from the right (Fig. 4). In life, the count would likely have been closer to 19 per side, as reported in *Gorgosaurus libratus* (Lambe, 1917). Each rib consists of a medial and lateral portion. The medial portions are elongate with spatulate heads that overlap about the midline. The ventral surface of each head bears a large, rugose attachment site for the adjoining rib head, which itself bears a smaller corresponding attachment site on the ventral surface. Each medial element quickly narrows laterally to form the rib shaft, which curves caudolaterally and slightly dorsally along its length. Approximately mid-way along the length of the rib shaft, an elongate facet occurs laterally for the attachment of the lateral gastralial element. These elements are largely missing, although a few preserved examples show them to be little more than slender bony rods. Moving caudally along the series, the gastralia

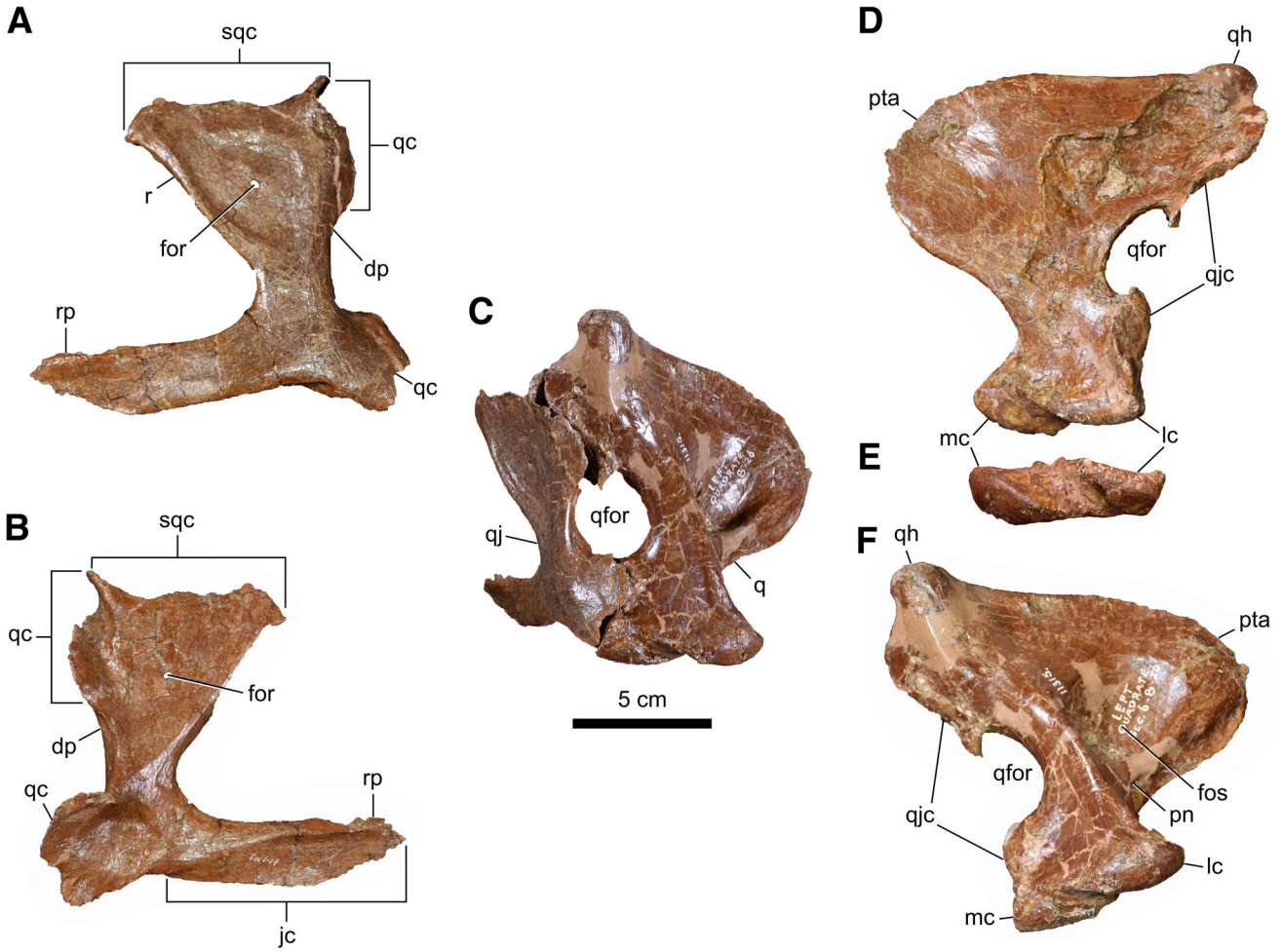

Fig. 2. Left suspensorial bones of CMN 11315. Quadratojugal in lateral (**A**) and medial (**B**) views. (**C**) Posterolateral view of the quadratojugal-jugal complex. Quadrate in rostral (**D**), ventral (**E**), and caudal (**F**) views. Abbreviations: rp, rostral process; dp, dorsal process; for, foramen; fos, fossa; jc, jugal contact; lc, lateral condyle; mc, medial condyle; pn, pneumatic fossa; pta, pterygoid ala; q, quadrate; qc, quadrate contact; qfor, quadrate foramen; qh, quadrate head; qj, quadratojugal; qjc, quadratojugal contact; r, ridge; sqc, squamosal contact.

decrease in size, with narrower heads and a more pronounced caudal curvature. The caudalmost gastralia are indistinguishably fused about the midline, forming an inverse U-shape. The individual gastralia are considerably less robust than reported in *Ty. rex* (Brochu, 2003) or *Ta. bataar* (Maleev, 1974).

Pectoral Girdle

The scapula (Fig. 5) is tightly appressed to the coracoid; the contact is open ventrally, but closed (with a visible suture) dorsally. The area of the acromion process of the scapula is badly damaged due to crushing, but field photos showing the outline of the comparatively intact element prior to removal (Fig. 5(E)) indicate that the process was not particularly well developed, being less than three times the minimum dorsoventral depth of the blade. The scapula is broken in two at midlength, but can be rejoined along a thin splint of bone ventrally; a large portion of the dorsal surface of the scapular blade is missing. The slender scapular blade is concave ventrally as in albertosaurines; the blade is approximately straight in *D. torosus* and *Ty. rex* (Russell, 1970; Brochu, 2003). The caudal end of the scapula is modestly expanded and broadly rounded, but it is doubtful whether this character is of taxonomic significance; in *G. libratus*, the caudal end of the scapula may be either slightly expanded and rounded (as in CMN 11315), or more widely expanded and squared off (Lambe, 1917; Matthew and Brown, 1923). In *D. torosus*, the caudal end of the scapula is slightly expanded and squared off (Russell, 1970), and in the only described postcranium of *A. sarcophagus*, it is broadly expanded and rounded (Parks, 1928). Variation in the caudal shape the scapula probably reflects variation in ossification of the scapular cartilage (Romer, 1956).

The quadrangular coracoid (Fig. 4) is weakly hooked at its anteroventral corner and broadly rounded, but, again, this character appears to be intraspecifically variable in *G. libratus* (Parks, 1928). The oval coracoid foramen, visible adjacent to the scapular contact medially, is obscured by local crushing of the lateral surface. The coracoid only contributes to approximately a quarter of the surface area of the humeral glenoid, which is reniform and faces ventrolaterally.

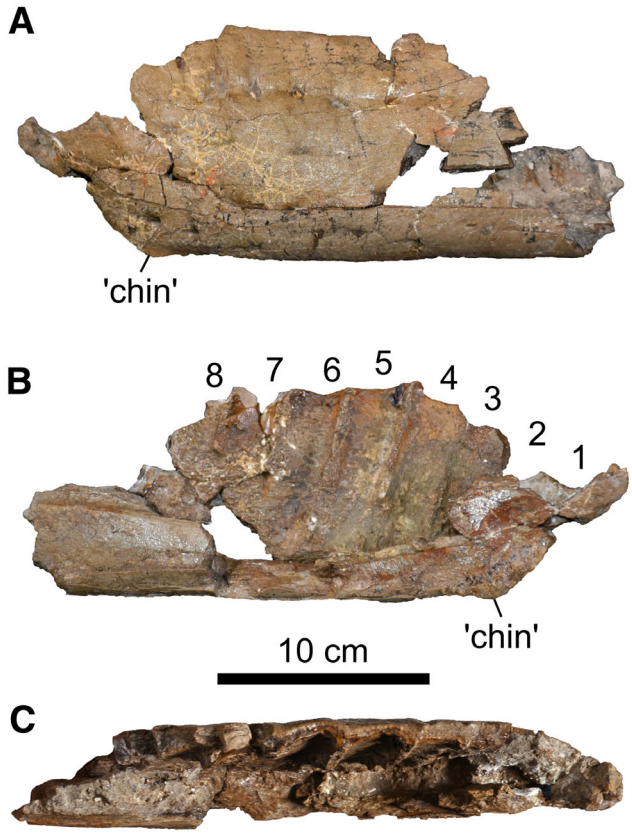

Fig. 3. Left dentary fragment of CMN 11315 in lateral (**A**), medial (**B**), and dorsal (**C**) views. Numbers indicate tooth positions.

Fig. 4. Gastralia of CMN 11315 in ventral view. The positions of the individual gastralia are approximate, based on their size and shape.

The furcula (Fig. 5D,E) was described in some detail by Makovicky and Currie (1998). It measures 163 mm transversely, with an interclavicular angle of 115 degrees. Compared with that of adult tyrannosaurids (e.g., *G. libratus*, TMP 1994.012.0602; *D. torosus*, CMN 8506), the furcula is slenderer with more poorly developed epicleideal facets.

Forelimb

The left humerus (Fig. 6) has suffered some crushing in the craniocaudal plane. It is 33% the length of the femur, which is comparable to relative lengths reported in *A. sarcophagus* and *D. torosus*, but shorter than those reported in *Ta. bataar* or *Ty. rex* (Sereno et al., 2009). The humeral head is low and poorly differentiated from the remainder of the humerus, which is typical of early tyrannosauroids; however, the head overhangs (albeit weakly) both the cranial and caudal surfaces, as in tyrannosaurids (Sereno et al., 2009). The deltopectoral crest, partially reconstructed with plaster, is not as pronounced as in mature *A. sarcophagus* (e.g., ROM 807). The apex of the crest is located approximately 39% along the length of the humerus from the proximal end. In most tyrannosaurids, this value is typically on the order of less than 25% (Sereno et al., 2009). There are no additional muscle tubera distal to the deltopectoral crest, which are clearly visible in *Ty. rex* (Brochu, 2003). In *A. sarcophagus* and "*R. kriegsteini*," the medial condyle of the distal end of the humerus reportedly expands farther than the lateral one (Brusatte et al., 2010), which does not appear to be the case in CMN 11315, in which the condyles are equidimensional. There are two small (~9 mm) bones at the distal end of the humerus, apressed to each condyle. That adjacent to the lateral condyle is roughly spherical, and the other, adjacent to the medial condyle, is rather amorphous, partially obscured by plaster. The latter may simply be a loose fragment of the damaged medial condyle. The spherical bone near the lateral condyle is not obviously from another other part of the skeleton, and is plausibly interpreted as a sesamoid bone (Gudmundsen and Østensen, 1987).

The relatively straight ulna (Fig. 7A,B) is 52% the length of the humerus. Even taking into account crushing of the medial surface of the element, the ulna is quite slender compared to that of mature *A. sarcophagus* (Parks, 1928) and particularly *Ty. rex* (Brochu, 2003). The olecranon process is modest in size. There are no obvious tuberosities on the shaft of the element, as reported in *Ty. rex* (Brochu, 2003).

The rod-like radius (Fig. 7C,D) is rather featureless, owing in part to mediolateral crushing of the main shaft. The proximal articulation for the humerus is D-shaped, with a flattened lateral contact for the ulna. The radius narrows slightly at midlength before expanding again distally. In *Ty. rex*, the shaft is typically twisted about its long axis so that the distal end is oriented transversely (Carpenter and Smith, 2001); however, this does not appear to be the

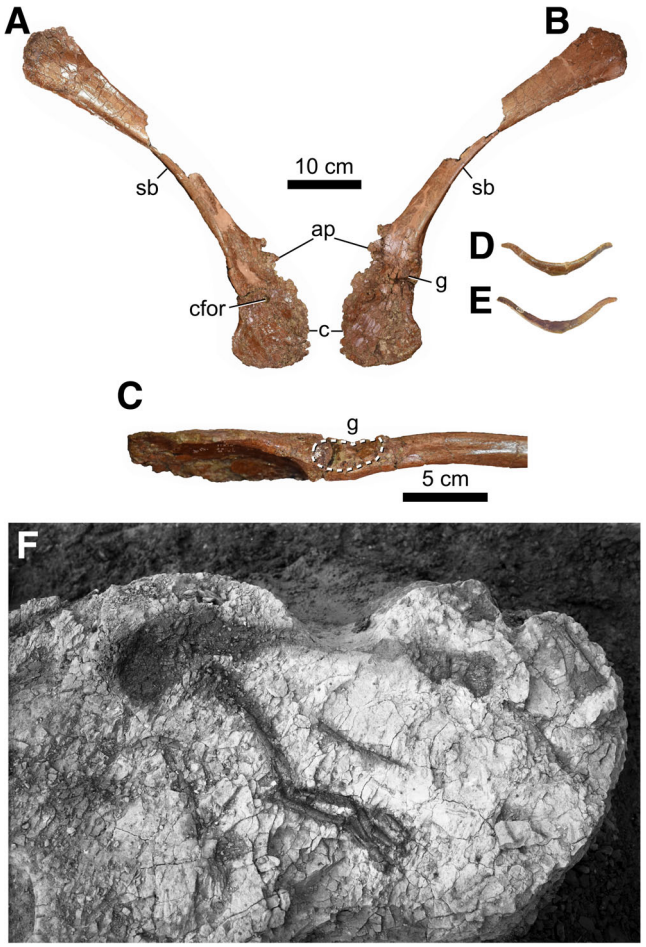

Fig. 5. Pectoral girdle of CMN 11315. Left scapulocoracoid in medial (**A**) and lateral (**B**) views. Close-up of glenoid (**C**). Furcula in anterior (**D**) and posterior (**E**) views. (**F**) Photograph of left pectoral girdle and forelimb in the field (CMN neg. 67947). Abbreviations: ap, acromion process (broken); c, coracoid; cfor, coracoid foramen; g, glenoid; sb, scapular blade.

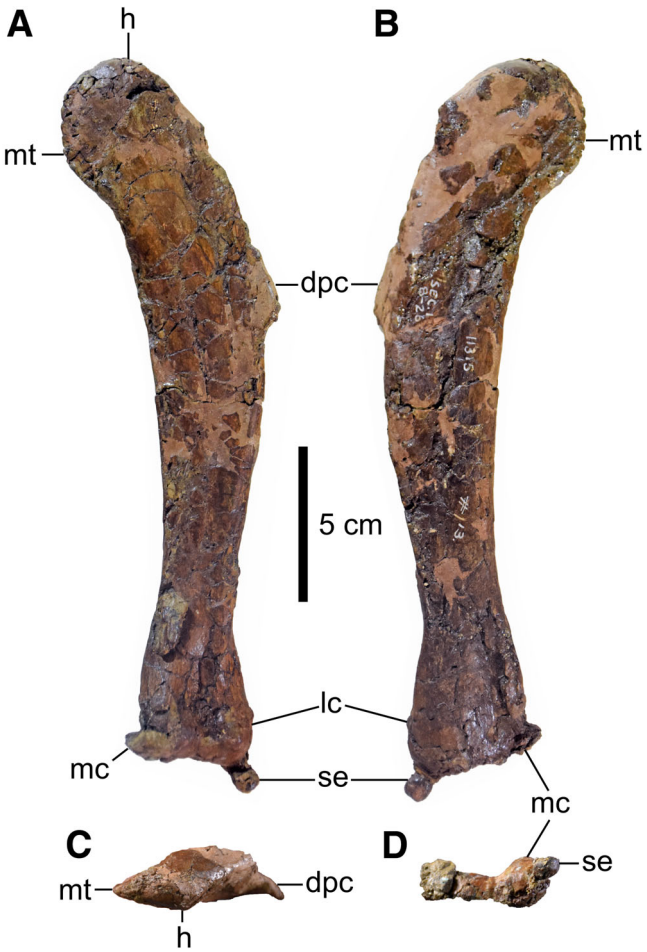

Fig. 6. Left humerus of CMN 11315 in cranial (**A**), caudal (**B**), dorsal (**C**), and ventral (**D**) views. Abbreviations: dpc, deltopectoral crest; h, humeral head; mc, medial condyle; mt, medial tubercle; lc, lateral condyle; se, sesamoid bone.

case in CMN 11315 or larger *A. sarcophagus* (ROM 807), in which the shaft is relatively straight along its length.

Three, possibly four, carpals are preserved. Their precise homologies are difficult to establish, given the varied interpretations that have been given from both neontological and palaeontological perspectives (Botelho et al., 2014; Xu et al., 2014). One carpal (Fig. 7C,D), shaped like a right triangle in distal outline, is associated with the distal end of the radius. It measures 11 mm wide × 9 mm long × 4 mm thick. It is interpreted as a scapholunare, a product of the fusion of the radiale and intermedium (Botelho et al., 2014). The largest carpal (Fig. 8A–C) straddles the proximal ends of metacarpals I and II, but does not completely overlap either. It is 14 mm wide × 12 mm long × 7 mm thick. The proximal surface, which has suffered some crushing, appears to bear a shallow, transversely oriented trochlea. This element has been interpreted as a "semilunate" carpal (Holtz Jr, 2000; Holtz Jr, 2004), and has also been reported in the basal tyrannosauroid *Guanlong wucaii* (Xu et al., 2006)—an identification with which we concur. However, in this case, the "semilunate" carpal appears to consist only of distal carpal 1, and is not a fusion of distal carpals 1 and 2 as reported elsewhere (Botelho et al., 2014). Rather, the smaller (9 mm wide × 5 mm long × 4 mm thick) distal carpal 2 (Fig. 8A,B) clearly lies immediately lateral to the "semilunate" carpal, centered proximal to metacarpal II. This arrangement goes to support the contention of Xu et al. (2014) that the "semilunate" carpal is not strictly homologous across all maniraptoriformes. The scapholunare and distal carpal 2 are markedly smaller than the semilunate carpal, whereas these elements are subequal in size in mature *A. sarcophagus* (ROM 807). There is possibly a fourth carpal (3–4 mm in all dimensions) apressed to the proximal end of metacarpal III, but this region is not particularly well preserved, so the perceived bone may be an artifact of crushing. If genuine, this element would likely represent distal carpal 3.

The metacarpals (Fig. 8B,C) are tightly apressed and preserved as a single block. The shaft of metacarpal I is wider than tall. The proximal articular surface is lunate, with a concave palmar surface. The distal condyles are greatly expanded dorsoventrally so that they are twice as

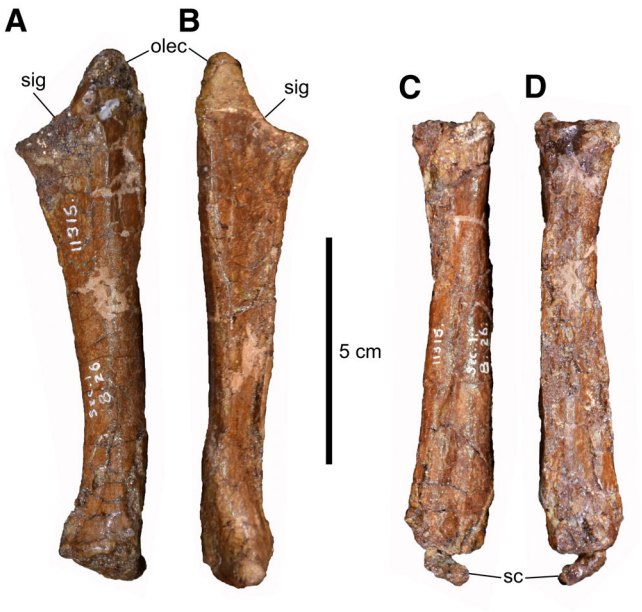

Fig. 7. Left forearm of CMN 11315. Ulna in lateral (**A**) and medial (**B**) views. Radius in lateral (**C**) and medial (**D**) views. Abbreviations: olec, olecranon process; sc, scapholunare; sig, sigmoid notch.

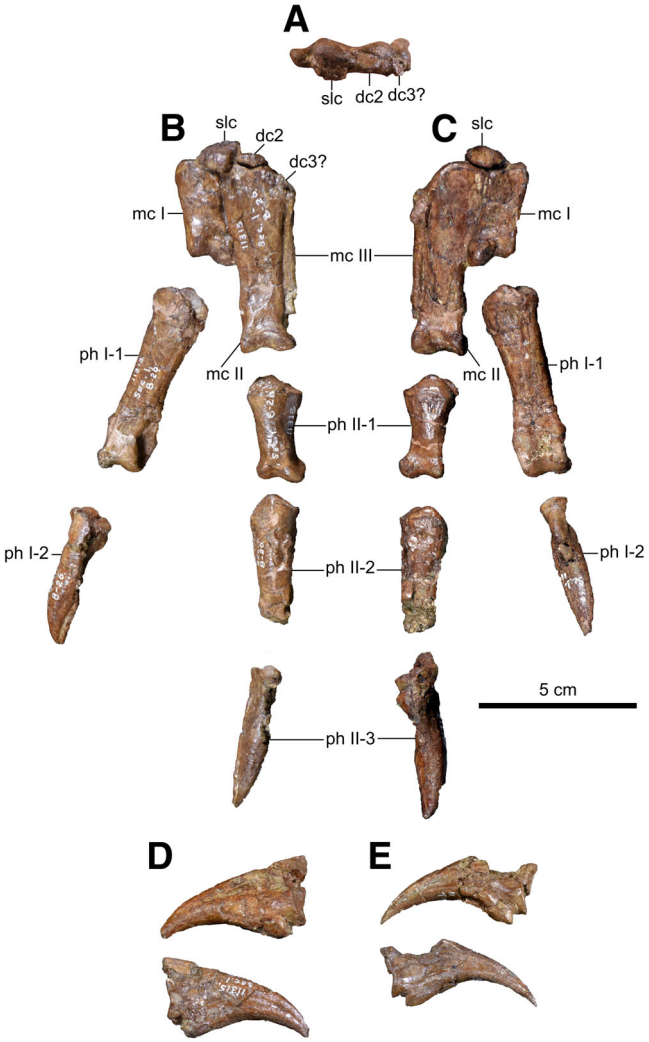

Fig. 8. Left wrist and manus of CMN 11315. Wrist elements in dorsal view (**A**). Manus in dorsal (**B**) and palmar (**C**) views. (**D**) Phalanx I-2 in medial (top) and lateral (bottom) views. Phalanx II-3 in medial (top) and lateral (bottom) views. Abbreviations: dc2, distal carpal 2; dc3, distal carpal 3; mc, metacarpal; ph, phalanx; slc, "semilunate" carpal.

deep here as elsewhere along the shaft. The lateral condyle extends farther distally than the medial one, forming an asymmetrical trochlea. This configuration would have restricted the first digit to operating at an angle of 15 degrees from the second one. The medial surface of the medial condyle is incised by a shallow ligament pit that is dorsally offset. Metacarpal II is 1.7 times longer than the first, and is slightly wider in the proximal half. The proximal articular surface is also lunate. The distal articular surface is more symmetrical than in the first metacarpal, although the lateral condyle is nevertheless slightly larger than the medial one. The shallow ligament pits on either side of the distal trochlea are centrally located compared to those of metacarpal I. Metacarpal III is a thin splint of bone that is intermediate in length between metacarpals I and II. The proximal articulating surface is deeper dorsoventrally, rather than mediolaterally as in the other two metacarpals. Metacarpal III does not reach as far proximally as metacarpals I and II, which has been a matter of small contention in the tyrannosaurid literature (Brochu, 2003). The proximal end of metacarpal III expands ventrally into a pointed tubercle, and the element gradually tapers distally before terminating in advance of the distal trochlea of metacarpal II. There is no distal trochlea on metacarpal III.

The manus is functionally didactyl, as only the first two digits are preserved (phalangeal formula = 2-3-0-X-X) (Fig. 8B,C). Phalanx I-1 is the longest element in the manus, being very slightly longer than metacarpal II. The proximal articular surface is deeply concave, with a subtle, medially offset ridge extending dorsoventrally; this shape corresponds well to that of the articulating trochlea of the adjoining metacarpal. The prominent dorsal and ventral rims of the proximal articulating surface ensure a firm articulation with metacarpal I. The shaft of phalanx I-1 is slightly concave ventrally. The distal trochlea is rotated clockwise about the long axis of the element, offset from the proximal articulating surface by approximately 25 degrees. The lateral condyle is slightly larger than the medial one, and the articular surface of the trochlea extends well onto the ventral surface of the phalanx, evidently more so than in *Ty. rex* (Brochu, 2003). The deep ligament pits are positioned centrally on either side of the trochlea. Phalanx I-2 is developed into a mediolaterally narrow, decurved ungual (Fig. 8B–D). The proximal articulating surface is teardrop-shaped, and is overhung dorsally by a subtle bony lip. The flexor tubercle, located proximoventrally, is modestly developed, less exaggerated than in early tyrannosauroids. The flexor margin of the claw is weakly concave; the ratio of the maximum height of the flexor margin to claw length (measured from flexor tubercle to claw tip) is 0.12. Deep grooves incise each side of the ungual, the medial groove being slightly more ventrally positioned than the lateral groove.

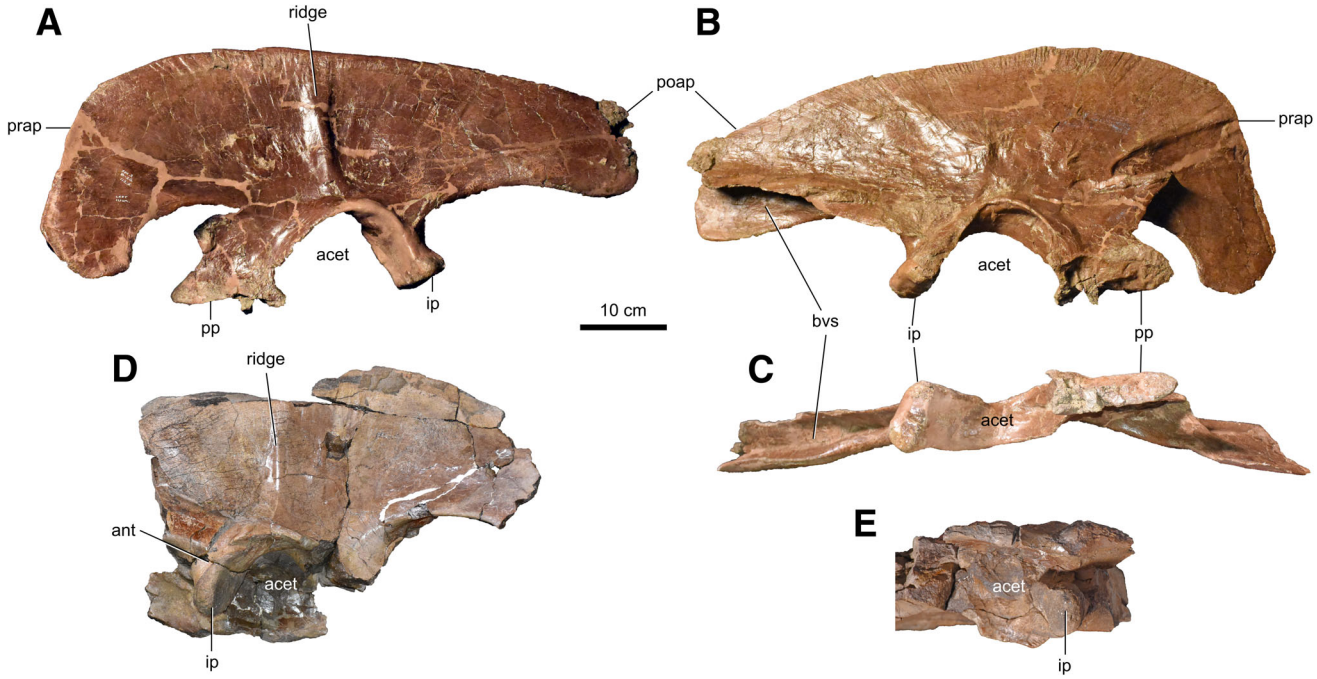

Fig. 9. Ilia of CMN 11315. Left ilium in lateral (**A**), medial (**B**), and ventral (**C**) views. Partial right ilium in lateral (**D**) and ventral (**E**) views. Abbreviations: acet, acetabulum; ant, antitrochanter; bvs, brevis shelf; ip, ischial peduncle; poap, postacetabular process; pp, pubic peduncle; prap, preacetabular process.

The non-ungual phalanges of digit II resemble phalanx I-1 in gross morphology, although they are considerably smaller and more robust. The distal trochlea of phalanx II-1 does not extend far onto the ventral surface of the element, and ligament pits are missing entirely. Phalanx II-2 is slightly longer than its proximal homologue, and the distal end is missing. Phalanx II-3 is again developed into a claw (Fig. 8B,C,E), albeit more gracile and more pointed than that of digit I. The flexor tubercle is slightly better defined than that of the ungual of digit I. The aforementioned measure of convexity is 0.21. The medial and lateral grooves are symmetrically positioned on the surface of the claw. Overall, the manual unguals are subequal in size, whereas in mature *A. sarcophagus* (e.g., ROM 807), the ungual of digit I is markedly larger than that of digit II.

Pelvic Girdle

The maximum length of the ilium (Fig. 9) is 98% the length of the femur. In most adult tyrannosaurids, this value is on the order of 105%–115% (Holtz Jr, 2001). There is a strong, anterodorsally extending ridge on the lateral surface of the iliac blade, dorsal to the acetabulum. This ridge is present in most tyrannosaurids except "*R. kriegsteini*" and *Qianzhousaurus sinensis* (Carr et al., 2017). The antitrochanter of the acetabular crest is very weakly developed, in contrast with those of early tyrannosauroids (Holtz Jr, 2001; Carr et al., 2017). The base of the pubic peduncle is much longer craniocaudally than the ischial peduncle, similar to the condition seen in the juvenile "*R. kriegsteini*" and early tyrannosauroids (Brusatte et al., 2010; Li et al., 2010). The ventral margin of the postacetabular process forms a subtle lobe, as in most tyrannosaurids except *Alioramus remotus*, *G. libratus*, *Q. sinensis*, and "*R. kriegsteini*" (Brusatte et al., 2010). The dorsal margin of the ilium is likewise convex cranially, and not flat along its entire margin as it is in "*R. kriegsteini*" and early tyrannosauroids (Brusatte et al., 2010).

The conjoined pubes (Fig. 10) are both broken at a third of their lengths and cannot be reassembled due to missing bone. There is evidently more bone missing from the left side. The pubic shaft is bowed caudally, unlike "*R. kriegsteini*" and early tyrannosauroids in which it bows cranially (Carr and Williamson, 2010; Carr et al., 2017). The pubic tubercle, present on the anterolateral face of the element, is low (15 mm) and projects laterally. It is not caudally bordered by heavy rugosities as it is in adult tyrannosaurids (Carr and Williamson, 2010).

The midshaft diameter of the ischium (Fig. 11) is less than half that of the pubis, as in adult tyrannosaurids, and in contrast with the condition of the juvenile "*R. kriegsteini*," in which the midshaft diameter of both bones is more nearly equal (Sereno et al., 2009). The ischial shaft is straight, as in *Alb. sarcophagus* and *Te. curriei* (Loewen et al., 2013).

Hindlimb

The femora (Fig. 12) are mostly complete, although some parts are missing, particularly about the midshaft. Regardless, they appear to be accurately restored, and much of the missing or distorted morphology on one element is intact on its counterpart. The proximal face of the femur is straight and oriented at an obtuse angle to the long axis of the shaft (i.e., dorsally or proximally inclined head), which contrasts with the condition in *D. torosus* and *Ty. rex*, in which this surface is concave (Brusatte and Carr, 2016). The trochanteric fossa, located caudally between the femoral head and greater trochanter,

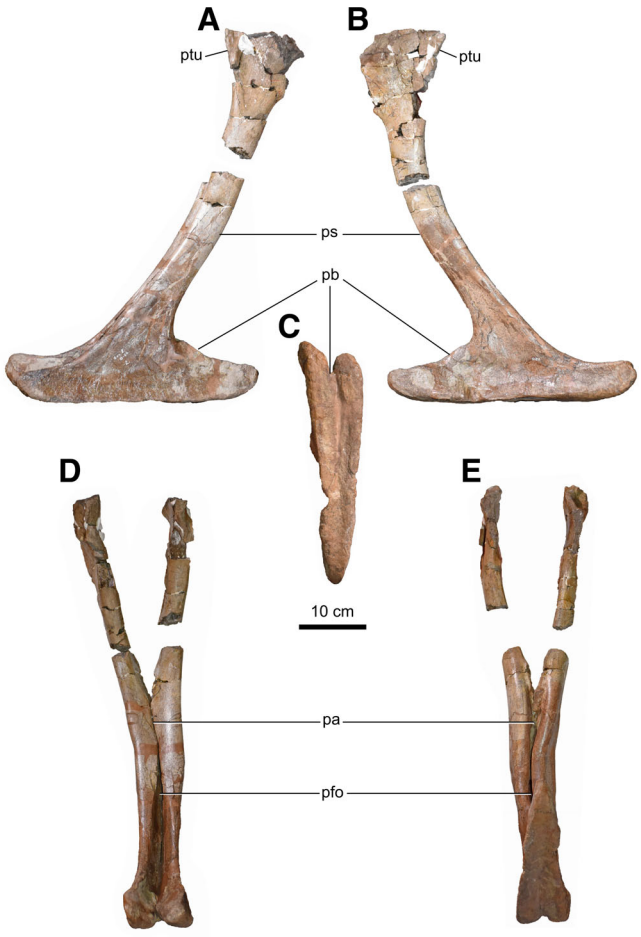

Fig. 10. Pubes of CMN 11315. (**A**) Left pubis in lateral view. (**B**) Right pubis in lateral view. (**C**) Pubic boot in ventral view. Pubes in cranial (**D**) and caudal (**E**) views. Abbreviations: pa, pubic apron; pb, pubic boot; pfo, pubic foramen; ps, pubic shaft; ptu, pubic tuberosity.

appears to be shallow, albeit somewhat obscured by local crushing. This is opposite the condition of many adult tyrannosaurids, in which the fossa is deep and triangular (Brusatte et al., 2012). The fourth trochanter is located 37.5% down the length of the femur, unlike in *D. torosus*, in which this value is less than 35% (Brusatte et al., 2010; Carr et al., 2017). There is a rough and oval muscle scar (52×27 mm^2; Fig. 12I) located caudally and slightly medially on the shaft, distal to the fourth trochanter, at about midlength. The scar is likely homologous to "ct1" reported by Brochu (2003) in *Ty. rex*, but is not displaced as far medially. A subtle ridge passes transversely across the proximal third of the scar, and may divide the insertion points for different bellies of the *M. adductor femoris* 2 (Carrano and Hutchinson, 2002).

The length of the tibia (Fig. 13) relative to the femur is approximately 1.02, which is close to the adult tyrannosaurid value of 1.00, and less than that reported for the juvenile "*R. kriegsteini*" (Sereno et al., 2009). There is no cranial process on the lateral condyle of the proximal end of the tibia, typical of early tyrannosauroids (Carr and Williamson, 2010). The cnemial crest is large, but it does not extend far proximally compared to the caudal condyles as it does in adult tyrannosaurids (Brusatte and Carr, 2016). The lateral malleolus of the distal tibia extends far laterally and further distally than the medial malleolus, and in these ways contrasts with the condition seen in *Ali. remotus*, where the lateral malleolus is less well developed (Brusatte et al., 2012). The iliofibularis tubercle of the laterally adjoining fibula (Fig. 13B–D,J) is bounded by a single crest laterally, rather than by two crests as in adult tyrannosaurids (Mader and Bradley, 1989; Carr et al., 2017). The astragalus (Figs. 13A,B,D,I and 14), tightly apressed to the anterodistal end of the tibia, closely resembles those of other tyrannosaurids in shape (Lambe, 1917; Parks, 1928; Brochu, 2003). A flat, subtriangular lateral distal tarsal bone caps the proximal end of the right metatarsal IV (Fig. 15C,E).

The pes (Figs. 15 and 16) differs from those of *B. sealeyi* and *D. horneri* in that the distal surface of metatarsal IV is approximately square in outline (it is craniocaudally elongate in the other two taxa) (Brusatte et al., 2010; Carr et al., 2017). Metatarsal IV also bears a proximodistally elongate, narrow muscle scar, located centrally along the shaft, and covering only a third of it (the scar is much wider and longer in *D. torosus* and *Ty. rex*) (Loewen et al., 2013). Also unlike these taxa, the proximal pedal phalanges are slender, having a length: width ratio greater than 3.0 (Brusatte et al., 2010).

OSTEOHISTOLOGICAL ANALYSIS

Methods

We attempted an osteohistological age assessment of CMN 11315 using a thin section from the distal third of the left fibula. This element was chosen because it was already broken and, because it is a non-weight-bearing bone, is arguably less likely to have remodeled the cortex with growth (Erickson et al., 2004; but see Chinsamy-Turan, 2005). Prior to cutting, we scanned the element in three-dimensions using a Go!Scan 20 handheld scanner and VXelements v. 6.1 software (Creaform, Lévis, Quebec). The 3D file and color 3D print are available at the CMN.

To produce the thin section, an ~5 mm-thick sample was cut using a Buehler Isomet 1000 Precision Saw. To remove saw marks and prepare it for mounting, the sample was lapped with a Hillquist 8 in lapidary using MetTech Silicon Carbide Grit in the sequence of 320 to 600 to 1,000. Once at the desired flatness, the sample was placed in a Fisher Scientific Ultrasonic Bath for 10–15 sec to remove grit and dust prior to mounting. The sample was then placed on a low heat Cole Parma Hotplate with the flat side up. When the sample was warm, Palouse Petropoxy 154 with hardener was applied to the flat surface, and a glass slide apressed to the epoxy, which was subsequently allowed to cure for 24 hr. The final thin section cut was made using the precision saw and thin section holder, producing a section of approximately 400–500 μm thick. A second round of lapping was conducted with 320 grit. Once close to desired thickness, 600-grit silicon carbide was used. Constant checking of the thin section with the microscope allowed determination of the desired thickness of approximately 30–35 μm. After this thickness was reached, polishing continued with 1,000 grit silicon carbide on a glass plate. The final polishing was done with 0.05 μm colloidal silica to obtain a sample surface suitable for SEM work. As a final step, the thin section was placed in the ultrasonic bath for 10–15 sec to remove any grit, colloidal silica, and dust from the sample.

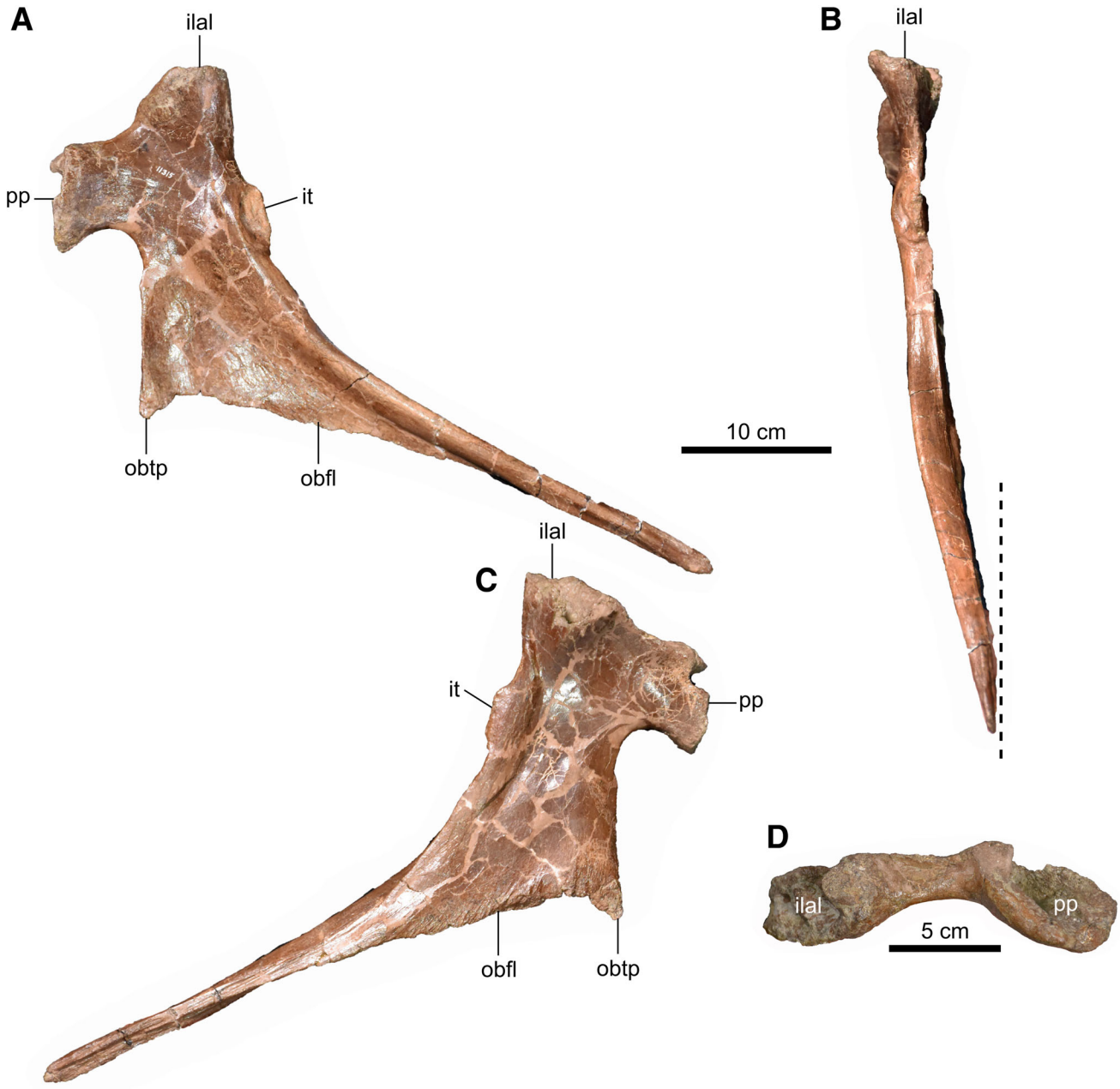

Fig. 11. Left ischium of CMN 11315 in lateral (**A**), caudal (**B**), and medial (**C**) views. (**D**) Close-up of peduncles in dorsal view. Abbreviations: ilal, ilac ala; it, ischial tuberosity; obfl, obturator flange; obtp, obturator process; pp, pubic process.

Large-area transmitted light microscopy image mosaics of the fibular section were acquired using a Zeiss AXIO Zoom.V16 light microscope. The mosaics were acquired with ZEN Pro software using the Plan Apo Z 1.0/0.25 objective (FWD 60 mm) at a resolution of 410 nm/pixel with plane-polarized and cross-polarized transmitted light. Each of the light microscopy image mosaic of the fibula thin section consists of 522 individual tiles.

A large-area SEM image mosaic of the fibular section was acquired with ZEISS Atlas 5 software using a ZEISS Gemini 450 FE-SEM at Fibics Incorporated (Ottawa, Canada). The large area light microscopy mosaics were imported into the respective Atlas 5 correlative workspace project, aligned with the sample in the SEM, and the large-area SEM image mosaic of the whole sample was imaged with an accelerating voltage of 20 kV simultaneously using the backscattered electron (BSE) detector, at a working distance of 9.917 mm, a 3.2 nA beam current, a 3 µsec dwell time, and a resolution of 65 nm/pixel. The resulting mosaics comprise 834 image tiles each, with each tile consisting of 10,240 × 10,240 pixels (666.7 × 666.7 µm), and a total pixel count of 87.5 gigapixels. Once the image mosaics were acquired, stitched, and corrected, the entire Atlas 5 data set was exported to an autonomous series of files called the

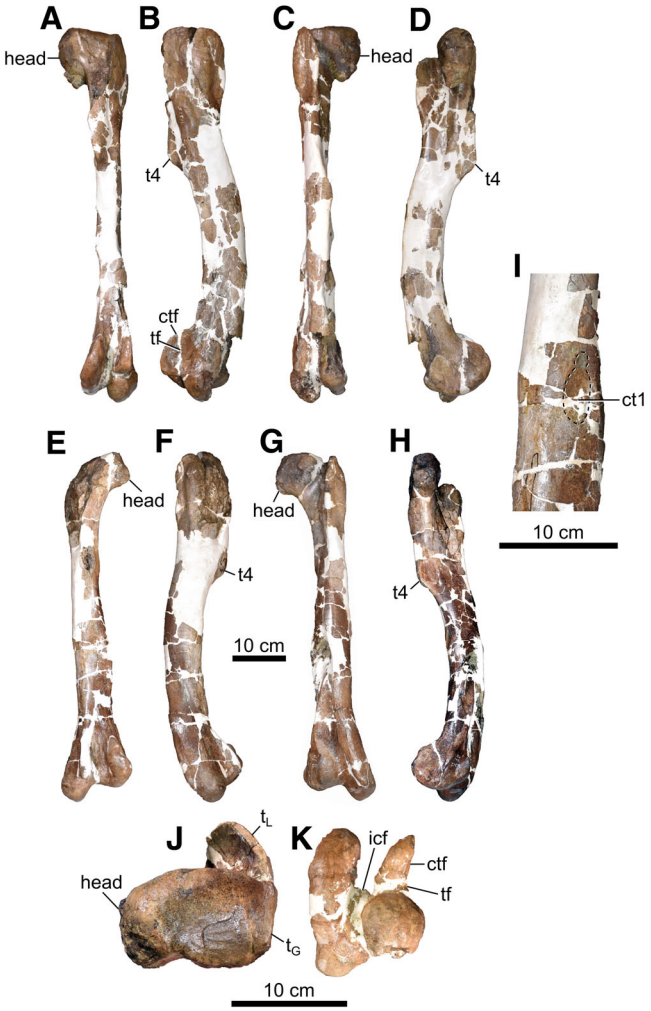

Fig. 12. Femora of CMN 11315. Right femur in caudal (**A**), lateral (**B**), cranial (**C**), medial (**D**), proximal (**J**), and distal (**K**) views. Left femur in caudal (**E**), lateral (**F**), cranial (**G**), and medial (**H**) views. (**I**) Close-up of shaft of left femur. Abbreviations: ctf, crista tibiofibularis; ct1, circular tuberosity on femur 1; icf, intercondylar fossa; tf, fibular trochlea; t_G, greater trochanter; t_L, lesser trochanter; t4, fourth trochanter.

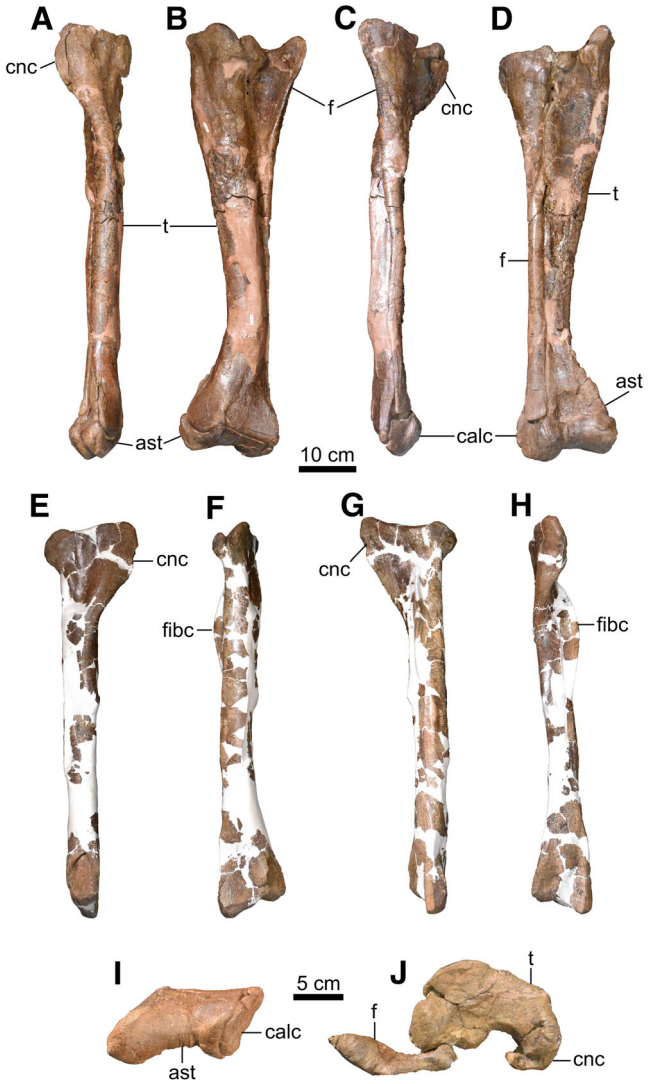

Fig. 13. Shin and tarsal elements of CMN 11315. Right shin elements in medial (**A**), caudal (**B**), lateral (**C**), cranial (**D**), and proximal (**J**) views. Left tibia in medial (**E**), caudal (**F**), lateral (**G**), and cranial (**H**) views. (**I**) Tarsal elements in ventral view. Left fibula not shown because it was sectioned for osteohistological analysis. Abbreviations: ast, astragalus; calc, calcaneum; cnc, cnemial crest; f, fibula; fibc, fibular crest; t, tibia.

Browser-Based Viewer (BBV), which allows anyone on a PC and a web browser to view the complete data set at full resolution in a similar manner to that of the Google Earth application. The computer mouse is used for zooming in and out as well as for navigating through the large area image mosaic. The BBV data sets of the fibula thin section can be viewed at the following link: http://www.petapixelproject.com/mosaics/museumofnature/TSB/TyrannosaurShinBone/index.html.

Results

The transverse thin section of the fibula (Fig. 17) is approximately D-shaped, with the flat surface facing medially, toward the tibia. The bone is dense, composed entirely of cortical tissue (i.e., lacking both a medullary cavity and spongiosa). Vascularization is longitudinal and occurs throughout the bone, most clearly demonstrated in the BSE SEM imagery. The cortex is zonal, the deepest zone making up ~70% of the section and being tan colored under plain

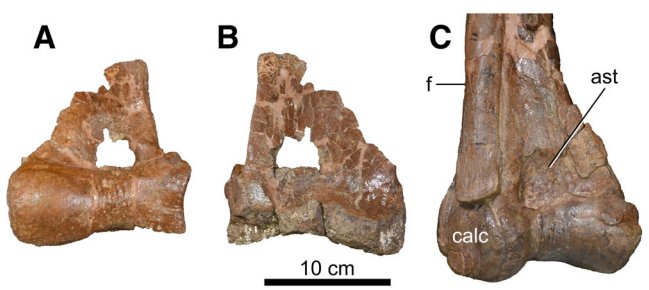

Fig. 14. Astragali of CMN 11315. Left astragalus in cranial (**A**) and caudal (**B**) views. (**C**) Right astragalus in cranial view. Abbreviations: ast, astragalus; calc, calcaneum; f, fibula.

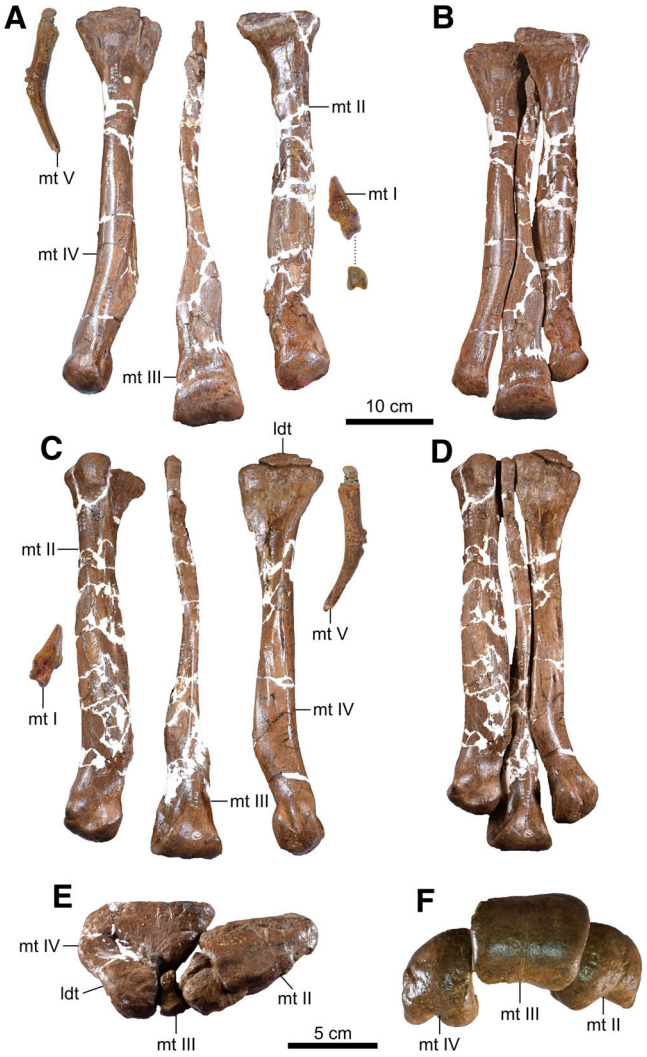

Fig. 15. Right metatarsus of CMN 11315. Cranial view exploded (**A**) and articulated (**B**). Caudal view exploded (**C**) and articulated (**D**). Articulated proximal (**E**) and distal (**F**) views. Articulated views include only metatarsals II–IV. (A) The distal articular end of metatarsal I at the end of the dotted line. Abbreviations: ldt, lateral distal tarsal; mt, metatarsal.

polarized light. Here, the primary bone is fibrolamellar with abundant primary osteons; however, remodeling is pervasive with overlapping secondary osteons scattered throughout, particularly toward the medial side. External to this, the cortical tissue is stained brown, and the zonation is somewhat finer, with three distinguishable zones of varying thickness. All three are composed of fibrolamellar primary tissue. The layers are separated by one or possibly two annuli, but it is difficult to trace them circumferentially because remodeling has obliterated the primary tissue medially. There is no sign of an external fundamental system near the periosteal surface.

MORPHOMETRIC ANALYSIS

Methods

Russell (1970) attributed CMN 11315 to *Daspletosaurus cf. D. torosus* based on the long humerus, radius-ulna, ilium, and circumference of the femur relative to femur length, all of which he argued are shorter in *Albertosaurus sarcophagus*. He also argued that ungual I-1 of CMN 11315 is less recurved than in *A. sarcophagus*, and that the metatarsus is slightly shorter than expected for the genus. However, although Russell did provide raw measurements for some tyrannosaurids, he did not otherwise show his work. Using the more extensive data set of Currie (2003a), we investigated the scaling relationships between log-transformed femur length and minimum shaft circumference, humeral length, radio-ulnar length, ilium length, and metatarsal III length for both albertosaurines (including *A. sarcophagus*) and tyrannosaurines (including *D. torosus*). The allometric series were subjected to analysis of covariance to assess the significance of differences between groups. Where significance was achieved ($\alpha = 0.05$), we calculated the distance (e_x) of CMN 11315 to both the albertosaurine and tyrannosaurine regression lines to determine with which clade it is most closely associated. All regressions and statistical analyses were conducted in PAST 3.15 (Hammer et al., 2001).

Results

Albertosaurines and tyrannosaurines are statistically indistinguishable with respect to both humerus and radius length; however, the two clades differ in the lengths of the ulna, ilium, metatarsal III, and in the circumference of the femur (Table 2). Proportionally, the ulna and ilium of CMN 11315 are more similar to those of albertosaurines, yet the specimen more closely resembles tyrannosaurines with respect to the proportions of metatarsal III and femur circumference (Fig. 18; Table 3).

PHYLOGENETIC ANALYSIS

Methods

We further assessed the phylogenetic affinities of CMN 11315 by scoring the specimen for 105 of 386 (27.2%) characters in the tyrannosauroid character matrix of Carr et al. (2017) (Supplementary Data 1). We conducted a parsimony-based cladistic analysis using the "traditional search" function in TnT v. 1.1 (Goloboff et al., 2008). The number of trees held in memory was set to the maximum (99,999). We used Wagner trees as starting trees with a random seed of 0, and specified 10,000 replicates with 1,000 trees saved per replicate. Tree bisection reconnection was retained as the swapping algorithm. Character ordering and taxon exclusion followed the specifications given in Carr et al. (2017), with the exception of including "*Raptorex kriegsteini*" to assess its placement and inferred maturity relative to CMN 11315. We also performed a second phylogenetic analysis, discounting ontogenetically variable characters by excluding all 49 ordered characters (*sensu* Currie et al., 2016); other variables were maintained as before.

Standard bootstrap values were calculated using 1,000 replicates, and reported as absolute frequencies. Bremer support was calculated using the Bremer.run script in TnT.

Results

The initial search returned 480 most parsimonious trees (MPTs) of 837 steps each (consistency index = 0.535, retention index = 0.804). The strict consensus tree was not particularly well resolved, so the 50% majority rule consensus

Fig. 16. Pedes of CMN 11315. (**A**) Right pes; (**B**) left pes; (**C**) right digit I ungual in medial (left) and lateral (right) views; (**D**) right digit IV ungual in medial (left) and lateral (right) views; (**E**) left digit II ungual in lateral (left) and medial (right) views; (**F**) left digit IV ungual in lateral (left) and medial (right) views. Roman numerals (I–IV) indicate digit numbers.

tree is shown in Figure 19 (left). CMN 11315 falls outside of Tyrannosauridae (*sensu* Brusatte and Carr, 2016), in a polytomy with *Appalachiosaurus montgomeriensis*, *Bistahieversor sealeyi*, *Dryptosaurus aquilunguis*, and an unnamed taxon from Iren Dabasu. It is slightly more derived than the recognized immature tyrannosaurid "*Raptorex kriegsteini*." Support for the least inclusive clade containing CMN 11315 and *T. rex* is low, with <50% bootstrap support and a Bremer support value of 0. Forcing CMN 11315 to be the sister taxon to Albertosaurinae (*Albertosaurus sarcophagus* + *Gorgosaurus libratus*) in Mesquite v. 3.04 (Maddison and Maddison, 2015) requires an additional step, and forcing it to be the sister taxon to *Al. sarcophagus* requires an additional two-steps. By contrast, forcing the same specimen to be the sister taxon to both *Daspletosaurus* spp. and *Da. torosus* requires 12 additional steps, and to *Da. horneri* requires 10 steps. CMN 11315 uniquely shares with Albertosaurinae a caudally concave ischium, and with *Al. sarcophagus* a lobe-like flange of the postacetabular process of the ilium.

The second phylogenetic analysis, excluding all ordered characters, produced 16 MPTs of 646 steps each. The strict consensus tree (CI = 0.470, RI = 0.805) (Fig. 19 right) recovered CMN 11315 as the sister taxon to Tyrannosauridae + (*B. sealeyi* + *Lythronax argestes*). Support for this grouping is again low (bootstrap <50%,

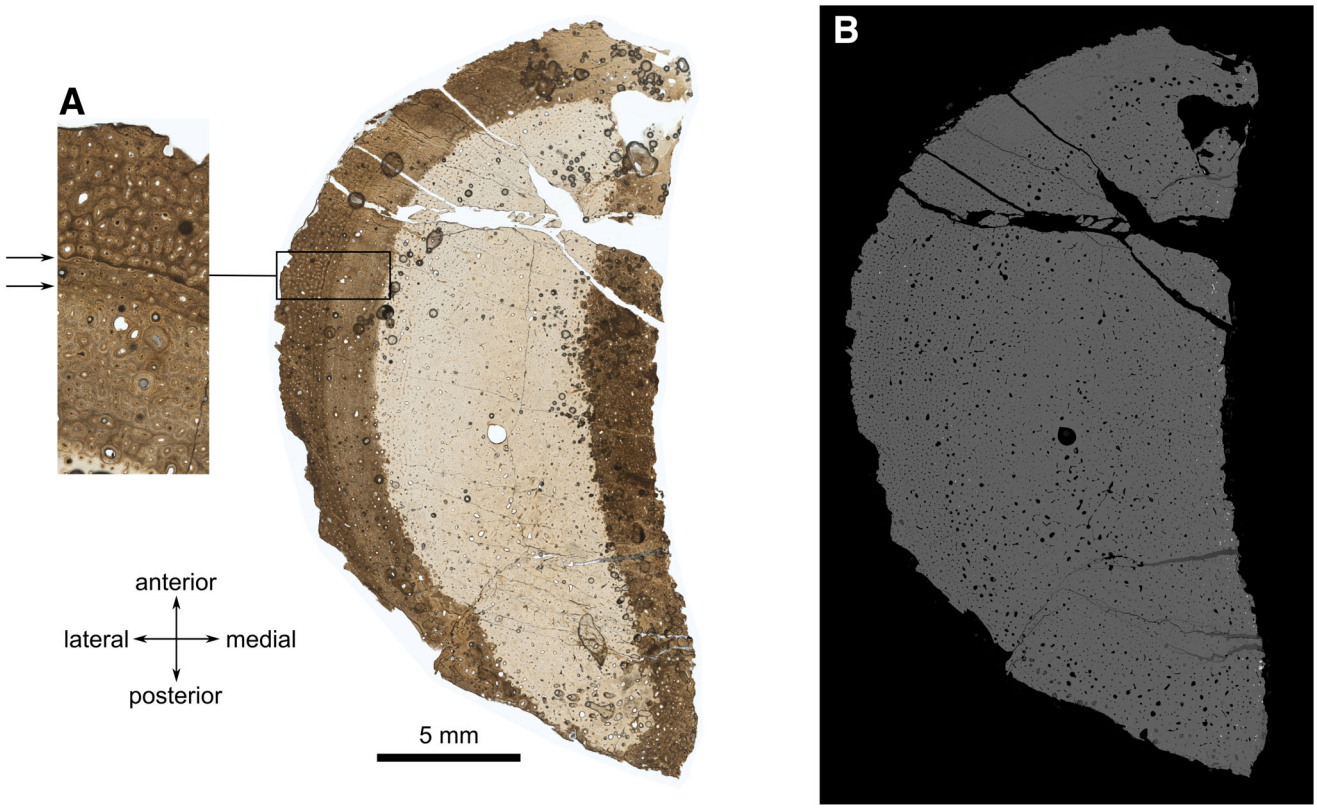

Fig. 17. Osteohistology of the left fibula of CMN 11315. (**A**) Thin section under plane-polarized light (inset shows possible growth lines, indicated by arrows); (**B**) large-area backscattered electron SEM image mosaic of the thin section showing bone porosity (see link to Atlas 5 BBV data set for high-resolution images).

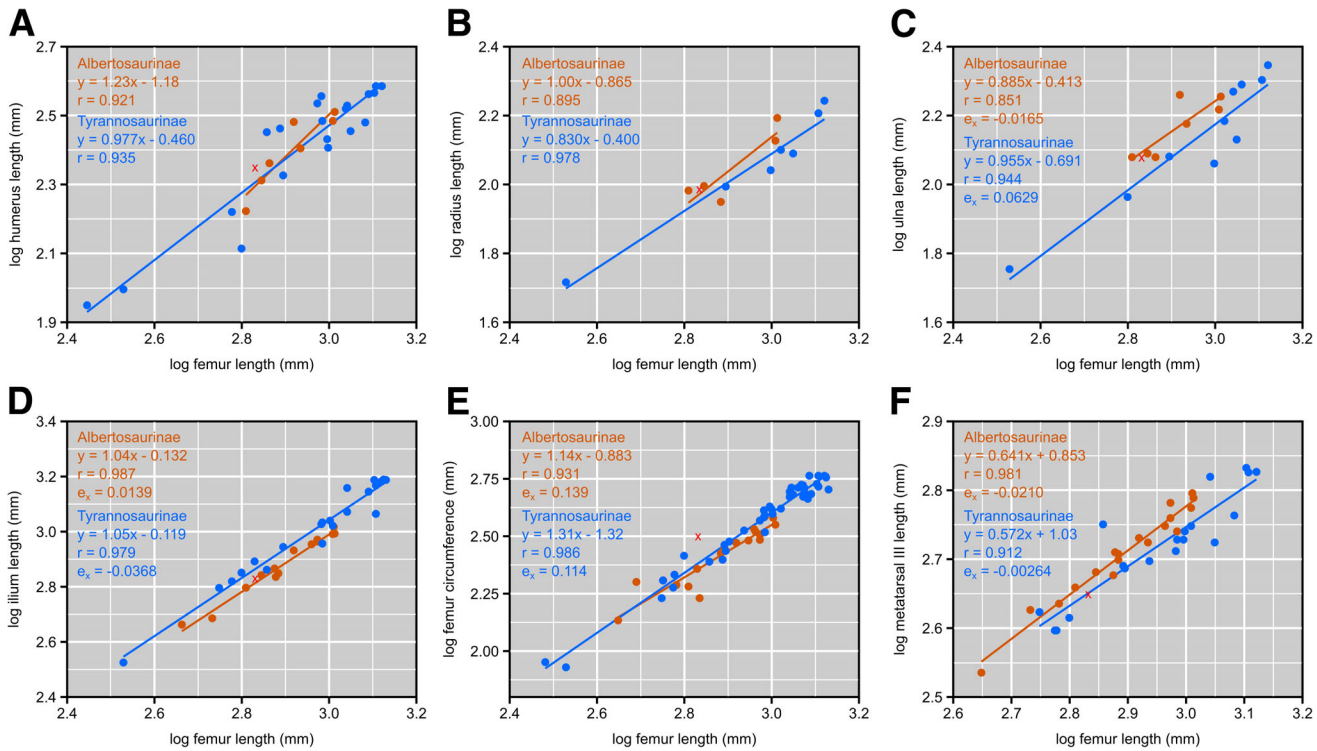

Fig. 18. Results of morphometric analyses. Regressions depict log-transformed humerus length (**A**), radius length (**B**), ulna length (**C**), ilium length (**D**), femur circumference (**E**), and metatarsal III length (**F**) plotted against log-transformed femur length for albertosaurines and tyrannosaurines. CMN 11315 indicated by the red X. e_x of CMN 11315 is given for those analyses of covariance (ANCOVA) in which significant differences were detected between albertosaurines and tyrannosaurines (see Table 2).

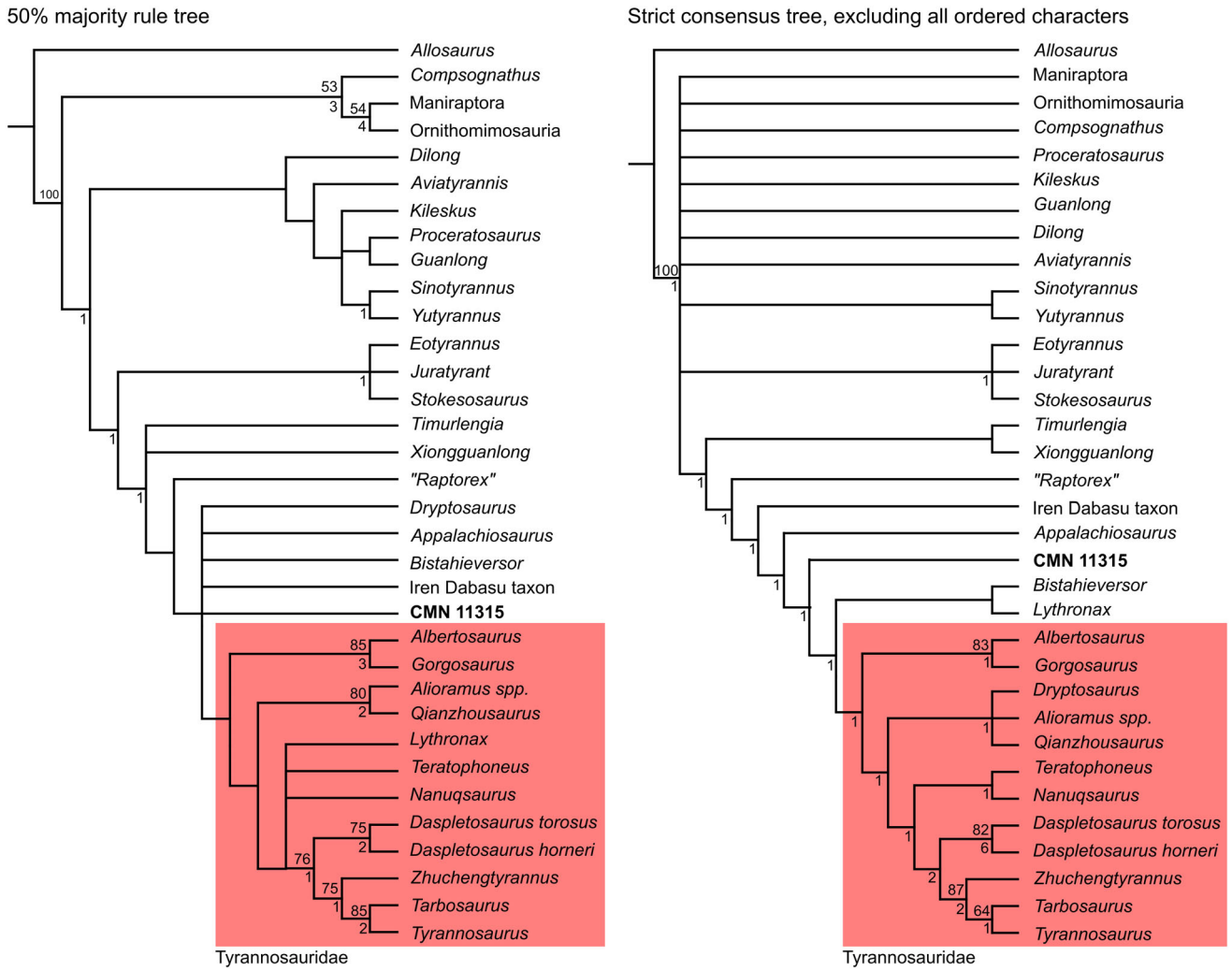

Fig. 19. Results of phylogenetic analyses. Tyrannosauridae highlighted in red. Numbers above nodes indicate bootstrap support; numbers below nodes indicate Bremer support.

Bremer support = 0). "*Raptorex kriegsteini*" was once again recovered as somewhat more basal. CMN 11315 shares the following synapomorphies with the clade Tyrannosauridae + (*B. sealeyi* + *L. argestes*): rotation of humeral shaft absent; concave notch between external tuberosity and deltopectoral crest absent; vertical linear ridge on lateral surface of ilium dorsal to acetabulum present; anterodorsal notch on ilium present; ventral margin of pubic boot straight; caudal surface of ischium concave; lateral distal condyle of femur with an cranial bulge that is slightly separated from the remainder of the condyle; and lateral malleolus of tibia extends significantly further distally than medial malleolus.

TABLE 2. ANCOVA results

	Slopes		Means	
Element	F-stat	*P* (same)	F-stat	*P* (same)
Femur circumference	2.73	0.104	9.664	**0.00291**
Metatarsal III	0.842	0.366	8.423	**0.00646**
Humerus	0.520	0.478	0.1316	0.720
Radius	0.437	0.527	1.744	0.219
Ulna	0.0486	0.829	6.864	**0.0202**
Ilium	0.0233	0.880	25.05	**1.82×10^{-5}**

Comparisons between Albertosaurinae and Tyrannosaurinae, using femur length as the independent variable. Significant *P*-values are given in bold.

DISCUSSION

Age of CMN 11315

CMN 11315 is evidently a subadult tyrannosaurid, based on its relatively small size (femur and ilium <750 mm long) and reduced muscle scarring; the latter generally becomes more pronounced with age. Fusion of the skull and vertebral bones is often used as an indicator of skeletal maturity (Hone et al., 2016), but unfortunately these are missing. Importantly, none of the aforementioned indicators of skeletal maturity are infallible, and supplementary osteohistological age assessment is typically advised when possible (Hone et al., 2016).

TABLE 3. Residual calculations for CMN 11315 from the albertosaurine and tyrannosaurine regression lines, using femur length as the independent variable

Element	Albertosaurinae		Tyrannosaurinae	
Ulna length	Observed	2.08	Observed	2.08
	Predicted	2.09	Predicted	2.01
	Residual (e_x)	**−0.0164**	Residual (e_x)	0.0629
Ilium length	Observed	2.83	Observed	2.83
	Predicted	2.82	Predicted	2.87
	Residual (e_x)	**0.0139**	Residual (e_x)	−0.0368
Femur circumference	Observed	2.50	Observed	2.50
	Predicted	2.36	Predicted	2.38
	Residual (e_x)	0.139	Residual (e_x)	**0.114**
Metatarsal III	Observed	2.65	Observed	2.65
	Predicted	2.67	Predicted	2.65
	Residual (e_x)	−0.0210	Residual (e_x)	**−0.00265**

Bolded values indicate the smaller residual and the likely affinity of CMN 11315.

Histology of the fibula of CMN 11315 shows that the animal was young and still growing when it died, indicated by the lack of prolific Haversian bone or of an external fundamental system. Thus, CMN 11315 is definitely not a "pygmy," as has been suggested for some small tyrannosaurid species (e.g., Bakker et al., 1988; Fiorillo and Tykoski, 2014). Notably, the age inferred from osteochronology (at least 2 years from counted annuli) is appreciably younger than that obtained from the tyrannosaurid growth curves of Erickson et al. (2004). Using development mass estimation (Erickson and Tumanova, 2000), and calibration data from Erickson et al. (2004), the inferred mass of CMN 11315, assuming it is *Albertosaurus sarcophagus*, is 501 kg. This corresponds to an age of ~13 years (Erickson et al., 2004). Similarly, if CMN 11315 is *Daspletosaurus* sp., the same method provides a mass estimate of 636 kg and an age of ~10 years. In either case, the animal plots within the exponential portion of its growth curve.

The age disparity between the osteochronological and growth curve estimates might be explained in one of two ways. First, it is possible that the complete growth record of CMN 11315 is not entirely reflected by the annuli, and that some growth marks (annuli or lines of arrested growth) are missing. This would not be terribly surprising, given that growth marks often vary in number between skeletal elements in any individual (Horner et al., 2000). Alternatively, it may be that the osteochronological age estimate is accurate, and that the logistic growth model of Erickson et al. (2004) is erroneous (Myhrvold, 2013). There may be some reason to suspect this, given that the model predicts almost no growth in the first five years of the animals' life. Regardless of the source of error, the point remains that CMN 11315 does not represent a skeletally mature individual.

Identity of CMN 11315

Although CMN 11315 is recovered as a non-tyrannosaurid tyrannosauroid in the cladogram, this unqualified identification is quite unlikely considering no such animal has ever been found in Upper Cretaceous strata of Laramidia (Brusatte and Carr, 2016). Almost certainly, this basal positioning is an upshot of the young ontogenetic age of CMN 11315, as it is lacking many of the relevant apomorphies that develop in adults (Gould, 1977). Such a phenomenon has been reported in tyrannosaurids elsewhere (e.g., Sereno et al., 2009; Tsuihiji et al., 2011), and is common in animals more widely (Hennig, 1999).

Accepting that CMN 11315 is a tyrannosaurid, the question remains as to which species it pertains. The historically varied classification of CMN 11315 as either *A. sarcophagus* (Madsen Jr, 1974; Holtz Jr, 2000; Currie, 2003b; Persons IV and Currie, 2016) or *Daspletosaurus* sp. (Russell, 1970; Makovicky and Currie, 1998; Currie, 2003a; Claessens, 2004; Nesbitt et al., 2009) makes sense in light of the equivocal morphometric results presented here. The specimen evidently shares a mix of features with both albertosaurines and tyrannosaurines. Importantly, although several of the albertosaurine and tyrannosaurine regression lines are significantly different, they are nonetheless often quite close, and the points overlap such that some plot closer to the opposite regression line. Thus, it is unsurprising that CMN 11315 should be variably allied with different taxa, particularly given the few variables considered here.

The greater number of variables included in the cladistic analysis might lead one to expect that it should provide a more exact identification, but this is not obviously the case. The number of plesiomorphic (and missing) character states is such that CMN 11315 falls outside of Tyrannosauridae, rather than with any particular taxon within it. Even so, the fewer steps necessary to unite CMN 11315 with *A. sarcophagus* than with *Daspletosaurus* spp. suggests that the former is a more parsimonious interpretation, all else being equal. Notably, CMN 11315 shares several skull characters (which are often considered the most useful for taxonomic identification; Currie et al., 2003) with *A. sarcophagus*, to the exclusion of tyrannosaurines. It shares only one (transition between the rostral and ventral margins of the dentary occurs below the first and second alveolus) with *Daspletosaurus* spp., to the exclusion of albertosaurines.

One must not be too careless with this phylogenetic line of reasoning. "*Raptorex kriegsteini*," a recognized juvenile *Tarbosaurus bataar* (Fowler et al., 2011; Tsuihiji et al., 2011), is also recovered outside of Tyrannosauridae, and (using the methods above) it takes ~50 fewer steps to unite it with any albertosaurine than with *T. bataar*. However, this does not mean that "*R. kriegsteini*" is instead an albertosaurine; biostratigraphic and biogeographic evidence strongly indicates that albertosaurines were not otherwise contemporaneous with "*R. kriegsteini*" (Brusatte and Carr, 2016). It is therefore imperative that

these additional considerations be brought to bear in such instances of taxonomic ambiguity.

To date, *A. sarcophagus* remains the only unequivocally identified tyrannosaurid species from the Horseshoe Canyon Formation (Carr, 2010; Eberth et al., 2013). *Daspletosaurus* spp. are otherwise known only from the older Dinosaur Park, Oldman, and Two Medicine formations (Currie, 2005; Carr et al., 2017). The presence of *Daspletosaurus* sp. as a second tyrannosaurid in the Horseshoe Canyon Formation, although not unprecedented (both *Daspletosaurus* sp. and *Gorgosaurus libratus* are present in the Dinosaur Park Formation; Farlow and Planka, 2002), requires more compelling evidence than that provided by Russell (1970), ideally in the form of a mature individual. Therefore, we consider the weight of the evidence, particularly the cladistic and biostratigraphic considerations, to favor the hypothesis that CMN 11315 represents an immature *A. sarcophagus.* Any morphometric similarity to *Daspletosaurus* spp. is attributable to convergent intraspecific variation.

CONCLUSIONS

Tyrannosauridae is rife with examples of species that have been coined on the basis of undiagnostic immature material, which has often led to overestimates of diversity (Currie and Dong, 2001; Currie, 2003b; Fowler et al., 2011). Although Russell (1970) did not name a new species specifically to receive CMN 11315, the effect of assigning it to *Daspletosaurus cf. D. torosus* was largely the same, in addition to artificially inflating the longevity of the genus. To be sure, accurate classification of immature skeletal material is often made quite difficult by the fact that diagnostic character states are typically not expressed until adulthood (Carr, 1999; Hone et al., 2016). Although none of the methods applied here was individually able to provide a satisfactory answer concerning the taxonomic status of CMN 11315, their combined application (in addition to historic and biostratigraphic considerations) yields a more definitive answer. We therefore stress the use of such "total evidence" approaches when taxonomic information is not forthcoming.

ACKNOWLEDGEMENTS

Thanks to P. Dodson and B. Hedricks for soliciting our contribution to this volume. Access to CMN 11315 was provided by M. Currie. Thin sectioning was completed by T. Mount. Photography of the specimen and manuscript formatting was done by S. Rufolo. Helpful discussion was provided by S. Brusatte and D. Hone. Constructive reviews were provided by editor P. Dodson, T. Carr, and an anonymous reviewer. This research was supported by a Discovery Grant to JCM from the Natural Sciences and Engineering Research Council of Canada.

LITERATURE CITED

Bakker RT, Williams M, Currie PJ. 1988. *Nanotyrannus*, a new genus of pygmy tyrannosaur, from the latest Cretaceous of Montana. Hunteria 1:1–30.

Botelho JF, Ossa-Fuentes L, Soto-Acuña S, Smith-Paredes D, Nuñez-León D, Salinas-Saavedra M, Ruiz-Flores M, Vargas AO. 2014. New developmental evidence clarifies the evolution of wrist bones in the dinosaur–bird transition. PLoS Biol 12:e1001957.

Brochu CA. 2003. Osteology of *Tyrannosaurus rex*: insights from a nearly complete skeleton and high-resolution computed tomographic analysis of the skull. J Vertebr Paleontol 22(Suppl 4): 1–138.

Brown CM, Ryan MJ, Evans DC. 2015. A census of Canadian dinosaurs: more than a century of discovery. In: ORP B-E, Powell GL, Jamniczky HA, Bauer AM, Theodor J, editors. *All Animals are Interesting: A Festschrift Celebrating the Career of Anthony P. Russell*. Oldenburg, Germany: BIS-Verlag der Carl von Ossietzky Universität. p 151–209.

Brusatte SL, Carr TD. 2016. The phylogeny and evolutionary history of tyrannosauroid dinosaurs. Sci Rep-UK 6:20252.

Brusatte SL, Norell MA, Carr TD, Erickson GM, Hutchinson JR, Balanoff AM, Bever GS, Choiniere JN, Makovicky PJ, Xu X. 2010. Tyrannosaur paleobiology: new research on ancient exemplar organisms. Science 329:1481–1485.

Brusatte SL, Carr TD, Norell MA. 2012. The osteology of *Alioramus*, a gracile and long-snouted tyrannosaurid (Dinosauria: Theropoda) from the Late Cretaceous of Mongolia. Bull Am Mus Nat Hist 366: 1–197.

Carpenter K. 1992. Tyrannosaurids (Dinosauria) of Asia and North America. In: Mateer NJ, Pei-Ji C, editors. *Aspects of nonmarine Cretaceous geology*. Beijing: China Ocean Press. p 250–268.

Carpenter K. 2002. Forelimb biomechanics of nonavian theropod dinosaurs in predation. Senck Leth 82:59–75.

Carpenter K, Smith M. 2001. Forelimb osteology and biomechanics of *Tyrannosaurus rex*. In: Tanke DH, Carpenter K, editors. *Mesozoic vertebrate life*. Bloomington: Indiana University Press. p 90–116.

Carr TD. 1999. Craniofacial ontogeny in Tyrannosauridae (Dinosauria, Coelurosauria). J Vertebr Paleontol 19:497–520.

Carr TD. 2010. A taxonomic assessment of the type series of *Albertosaurus sarcophagus* and the identity of Tyrannosauridae (Dinosauria, Coelurosauria) in the *Albertosaurus* bonebed from the Horseshoe Canyon Formation (Campanian–Maastrichtian, Late Cretaceous). Can J Earth Sci 47:1213–1226.

Carr TD, Williamson TE. 2010. *Bistahieversor sealeyi*, gen. et sp. nov., a new tyrannosauroid from New Mexico and the origin of deep snouts in Tyrannosauroidea. J Vertebr Paleontol 30:1–16.

Carr TD, Varricchio DJ, Sedlmayr JC, Roberts EM, Moore JR. 2017. A new tyrannosaur with evidence for anagenesis and crocodile-like facial sensory system. Sci Rep-UK 7:44942.

Carrano MT, Hutchinson JR. 2002. Pelvic and hindlimb musculature of *Tyrannosaurus rex* (Dinosauria: Theropoda). J Morphol 253: 207–228.

Chinsamy-Turan A. 2005. *The microstructure of dinosaur bone: deciphering biology with fine-scale techniques*. Baltimore: Johns Hopkins University Press.

Claessens LP. 2004. Dinosaur gastralia; origin, morphology, and function. J Vertebr Paleontol 24:89–106.

Currie PJ. 2003a. Allometric growth in tyrannosaurids (Dinosauria: Theropoda) from the upper Cretaceous of North America and Asia. Can J Earth Sci 40:651–665.

Currie PJ. 2003b. Cranial anatomy of tyrannosaurid dinosaurs from the Late Cretaceous of Alberta. Canada Acta Palaeontol Pol 48:191–226.

Currie PJ. 2005. Theropods, including birds. In: Currie PJ, Koppelhus EB, editors. *Dinosaur Provincial Park: a spectacular ancient ecosystem revealed*. Bloomington: Indiana University Press. p 367–397.

Currie PJ, Dong Z-M. 2001. New information on *Shanshanosaurus huoyanshanensis*, a juvenile tyrannosaurid (Theropoda, Dinosauria) from the Late Cretaceous of China. Can J Earth Sci 38:1729–1737.

Currie PJ, Trexler D, Koppelhus EB, Wicks K, Murphy N. 2005. An unusual multi-individual tyrannosaurid bonebed in the Two Medicine Formation (Late Cretaceous, Campanian) of Montana (USA). In: Carpenter K, editor. *The carnivorous dinosaurs*. Bloomington: Indiana University Press. p 313–324.

Currie PJ, Hurum JH, Sabath K. 2003. Skull structure and evolution in tyrannosaurid dinosaurs. Acta Palaeontol Pol 48: 227–234.

Currie PJ, Holmes RB, Ryan MJ, Coy C. 2016. A juvenile chasmosaurine ceratopsid (Dinosauria, Ornithischia) from the Dinosaur

Park Formation, Alberta, Canada. J Vertebr Paleontol 36: e1048348.
Eberth DA, Evans DC, Brinkman DB, Therrien F, Tanke DH, Russell LS. 2013. Dinosaur biostratigraphy of the Edmonton Group (Upper Cretaceous), Alberta, Canada: evidence for climate influence. Can J Earth Sci 50:701–726.
Erickson GM, Tumanova TA. 2000. Growth curve of *Psittacosaurus mongoliensis* Osborn (Ceratopsia: Psittacosauridae) inferred from long bone histology. Zool J Linn Soc-Lond 130:551–566.
Erickson GM, Makovicky PJ, Currie PJ, Norell MA, Yerby SA, Brochu CA. 2004. Gigantism and comparative life-history parameters of tyrannosaurid dinosaurs. Nature 430:772–775.
Farlow JO, Planka ER. 2002. Body size overlap, habitat partitioning and living space requirements of terrestrial vertebrate predators: implications for the paleoecology of large theropod dinosaurs. Hist Biol 16:21–40.
Fiorillo AR, Tykoski RS. 2014. A diminutive new tyrannosaur from the top of the world. PLoS One 9:e91287.
Fowler DW, Woodward HN, Freedman EA, Larson PL, Horner JR. 2011. Reanalysis of "*Raptorex kriegsteini*": a juvenile tyrannosaurid dinosaur from Mongolia. PLoS One 6:e21376.
Goloboff PA, Farris JS, Nixon KC. 2008. TNT, a free program for phylogenetic analysis. Cladistics 24:774–786.
Gould SJ. 1977. *Ontogeny and phylogeny*. Cambridge: Harvard University Press.
Gudmundsen TE, Østensen H. 1987. Accessory ossicles in the elbow. Acta Paediatr Scand 58:130–132.
Hammer Ø, Harper DAT, Ryan PD. 2001. PAST: Paleontological statistics software package for education and data analysis. Palaeontol Electron 4(1):4. http://palaeo-electronica.org/2001_1/past/issue1_01.htm.
Hennig W. 1999. *Phylogenetic systematics*. Davis DD, Zangerl R (translators). Champaign: University of Illinois Press.
Holtz TR Jr. 2000. A new phylogeny of the carnivorous dinosaurs. GAIA 15:5–61.
Holtz TR Jr. 2001. The phylogeny and taxonomy of the Tyrannosauridae. In: Tanke DH, Carpenter K, editors. *Mesozoic vertebrate life*. Bloomington: Indiana University Press. p 64–83.
Holtz TR Jr. 2004. Tyrannosauroidea. In: Weishampel DB, Dodson P, Osmólska H, editors. *The Dinosauria*. 2nd ed. Berkeley: University of California Press. p 111–136.
Hone DW, Farke AA, Wedel MJ. 2016. Ontogeny and the fossil record: what, if anything, is an adult dinosaur? Biol Lett 12:20150947.
Horner JR, De Ricqlès A, Padian K. 2000. Long bone histology of the hadrosaurid dinosaur *Maiasaura peeblesorum*: growth dynamics and physiology based on an ontogenetic series of skeletal elements. J Vertebr Paleontol 20:115–129.
Hurum JH, Sabath K. 2003. Giant theropod dinosaurs from Asia and North America: skulls of *Tarbosaurus bataar* and *Tyrannosaurus rex* compared. Acta Palaeontol Pol 48:161–190.
Lambe LM. 1917. The Cretaceous theropodous dinosaur *Gorgosaurus*. Mem Geo Surv Can 100:1–84.
Larson P. 2013. The case for *Nanotyrannus*. In: Parrish JM, Molnar RE, Currie PJ, Koppelhus EB, editors. *Tyrannosaurid Paleobiology*. Bloomington: Indiana University Press. p 15–53.
Li D, Norell MA, Gao KQ, Smith ND, Makovicky PJ. 2010. A longirostrine tyrannosauroid from the Early Cretaceous of China. Proc R Soc B-Biol Sci 277:183–190.
Lipkin C, Carpenter K. 2008. Looking again at the forelimb of *Tyrannosaurus rex*. In: Larson P, Carpenter K, editors. *Tyrannosaurus rex: The tyrant king*. Bloomington: Indiana University Press. p 166–190.
Loewen MA, Irmis RB, Sertich JJ, Currie PJ, Sampson SD. 2013. Tyrant dinosaur evolution tracks the rise and fall of Late Cretaceous oceans. PLoS One 8:e79420.
Maddison WP, Maddison DR. 2015. Mesquite: a modular system for evolutionary analysis. Version 3.04, Retrieved from: http://mesquiteproject.org.
Mader BJ, Bradley RL. 1989. A redescription and revised diagnosis of the syntypes of the Mongolian tyrannosaur *Alectrosaurus olseni*. J Vertebr Paleontol 9:41–55.
Madsen JH Jr. 1974. A new theropod dinosaur from the Upper Jurassic of Utah. J Paleontol 48:27–31.
Makovicky PJ, Currie PJ. 1998. The presence of a furcula in tyrannosaurid theropods, and its phylogenetic and functional implications. J Vertebr Paleontol 18:143–149.
Maleev EA. 1974. Gigantic carnosaurs of the family Tyrannosauridae. Jt. Sov.-Mong. Paleontol. Exped. Trans. [Russian] 1:132–191.
Matthew WD, Brown B. 1923. Preliminary notices of skeletons and skulls of Deinodontidae from the Cretaceous of Alberta. Am Mus Novit 89:1–10.
Myhrvold NP. 2013. Revisiting the estimation of dinosaur growth rates. PLoS One 8:e81917.
Nesbitt SJ, Turner AH, Spaulding M, Conrad JL, Norell MA. 2009. The theropod furcula. J Morphol 270:856–879.
Parks WA. 1928. Albertosaurus arctunguis: a new species of therapodous dinosaur from the Edmonton Formation of Alberta. Univ Toronto Studies, Geol Ser 25:1–42.
Persons WS IV, Currie PJ. 2016. An approach to scoring cursorial limb proportions in carnivorous dinosaurs and an attempt to account for allometry. Sci Rep-UK 6:19828.
Romer AS. 1956. *Osteology of the reptiles*. Chicago: University of Chicago Press.
Russell DA. 1970. Tyrannosaurs from the Late Cretaceous of western Canada. Natl Mus Nat Sci, Publ Palaeontol 1:1–34.
Russell DA. 1984. A check list of the families and genera of North American dinosaurs. Syllogeus 53:1–35.
Ryan MJ, Russell AP. 2001. Dinosaurs of Alberta (exclusive of Aves). In: Tanke DH, Carpenter K, editors. *Mesozoic vertebrate life*. Bloomington: Indiana University Press. p 279–297.
Sereno PC, Tan L, Brusatte SL, Kriegstein HJ, Zhao X, Cloward K. 2009. Tyrannosaurid skeletal design first evolved at small body size. Science 326:418–422.
Tanke DH, Currie PJ. 2010. A history of *Albertosaurus* discoveries in Alberta, Canada. Can J Earth Sci 47:1197–1211.
Tsuihiji T, Watabe M, Tsogtbaata K, Tsubamoto T, Barsbold R, Suzuki S, Lee AH, Ridgely RC, Kawahara Y, Witmer LM. 2011. Cranial osteology of a juvenile specimen of *Tarbosaurus bataar* (Theropoda, Tyrannosauridae) from the Nemegt Formation (Upper Cretaceous) of Bugin Tsav, Mongolia. J Vertebr Paleontol 31: 497–517.
Vance T. 1989. Probable use of the vestigial forelimbs of the tyrannosaurid dinosaurs. Bull Chicago Herpetol Soc 24:41–47.
Weishampel DB, Dodson P, Osmólska H. 2004a. *The Dinosauria*. 2nd ed. Berkeley: University of California Press.
Weishampel DB, Barrett PM, Coria RA, Le Loeuff J, Xu X, Zhao X, Sahni A, Gomani EMP, Noto CR. 2004b. Dinosaur distribution. In: Weishampel DB, Dodson P, Osmólska H, editors. *The Dinosauria*. 2nd ed. Berkeley: University of California Press. p 517–606.
Xu X, Clark JM, Forster CA, Norell MA, Erickson GM, Eberth DA, Jia C, Zhao Q. 2006. A basal tyrannosauroid dinosaur from the Late Jurassic of China. Nature 439:715–718.
Xu X, Han F, Zhao Q. 2014. Homologies and homeotic transformation of the theropod 'semilunate' carpal. Sci Rep-UK 4:6042.